





---

## Master - Thesis

### Geoecology

**Assessment of the soil water balance and irrigation recharge  
by combination of cosmic ray neutron sensing  
and eddy covariance technique  
on a citrus orchard in the Haouz plain, Morocco.**

Katja Mroos

Matriculation number: 763691

katja.mroos@gmx.de

25.04.2014

Supervisors:

1. Dr. Gabriele Baroni

Institute of Earth and Environmental Sciences, University of Potsdam

2. Prof. Salah Er-Raki

Faculty of Sciences and Techniques, Cadi Ayyad University of Marrakesh



عندما تكون البئر فارغة، يتعلم المرء أن يقدر الماء



## Acknowledgments

Writing a thesis in another country and another culture is not possible without the help of several people, giving their knowledge, courage and hospitality to one. I first want to thank everybody who made it possible that I had the chance to go to Morocco: the University of Potsdam, the University of Marrakesh and the federal ministry of education (BMBF) for financing this project.

Thanks for an intensive time with a lot of extraordinary experiences, an increase in knowledge, the feeling to be a part of another culture and that I got the trust to handle this project. To my first supervisor, Dr. Gabriele Baroni, a great thank for his fruitful, helping and always inspiring supervision due to the easier and harder ways of my thesis time. By his open and friendly nature he always gave me a feeling of motivation and understanding.

Thanks to Prof. Salah Er-Raki, my second supervisor from the University of Marrakesh. He supported me during my stays in Marrakech with the organization of my field trips and the data I needed for my thesis. I would also like to thank Prof. Lahoucine Hanich for his support in organizing everything during my stay like the field trips, the laboratory, the housing and much more. There always was the possibility to ask for help, discuss problems or get support for all my requests.

I would like to thank Prof. Sascha Oswald and Dr. Till Franke for their support while preparation of my stays in Morocco and for fruitful discussions and suggestions in the process of writing. It was always possible to contact you and to have your ear and understanding.

Thanks to the team of the Laboratoire Mixte International TREMA for their help at field work and needful data support and helpful discussions of my results. A special thanks to Adrien, who welcomed me two times with an incredible hospitality in his cozy flat and for the time he spend with me. Thank you again so much.

Je remercie tout particulièrement Simo qui nous a accueilli, Klemens et moi et s'est occupé de nous. Il nous a beaucoup éclairé sur notre travail en nous communiquant ses motivations et ses compétences. Sans lui, notre travail à Agafay aurait été de bien moindre qualité et aurait eu du mal à aboutir.

A great thank to Klemens who helped me two times in the field, in bad-tempered moments, who was a perfect travelling partner and friend. During the time of writing I always felt that I was in good hands and experienced help and friendliness from my office neighbours in house 1.

For the introduction to the method and the field work of cosmic ray sensing and a great helpfulness I would like to thank Dr. Carlos Rivera Villarreyes.

Thanks to my friends who helped me preparing my field trips, gave fruitful hints while writing and prevented me from finishing this thesis to fast. Thanks Anja, Anna, Lena, Ulli, Matze, Theo, Klemens, Lukas, Aline, Georg, David, Josi, Sandra.

Thanks to the interest and patience of the proofreaders. You did a great job. Everybody.

Am Ende möchte ich vor allem meinen Eltern danken, die mich während der gesamten Zeit des Studiums sehr unterstützt haben und Geduld mit meinen Ansichten und Meinungen gezeigt haben. Ich weiß dies sehr zu schätzen und danke euch für euer entgegengebrachtes Vertrauen.



---

## Abstract

In the last 50 years resource-intensive agriculture, increasing high-end tourism and extensive urbanism lead to an alarming depletion (up to 50 m beneath surface) of the ground water table in the region around Marrakesh (Morocco). At given climatical conditions and constant anthropogenic overexploitation the possibilities for a natural groundwater recharge are restricted.

By a quantification of the artificial groundwater recharge by excess drip irrigation is conducted for a 50 ha citrus orchard, 30 km southwest of Marrakesh. For this aim, a soil water balance is set up from June to December 2013. By combining the eddy covariance technique (ECT) and the cosmic ray sensing (CRS), the calculation of the soil water balance on field-scale is possible. ECT determines the actual evapotranspiration on field-scale in high-resolute time steps. CRS is used for the calculation of soil moisture by the inverse relation between cosmic neutrons and hydrogen in the soil for an area of about 30 ha. Particularly in regard to heterogeneous soil moisture conditions the capability of CRS is assessed. Inhomogeneous soil conditions, due to linear arranged tree rows with drip irrigation, make a modification of the calibration procedure necessary. Vertical and horizontal irregularities in soil moisture are considered by a weighting of the calibration dataset. Comparative measurements from TDR, evaporimeter and fluxmeter are used to validate the results of ECT and CRS.

The adaptation of the calibration procedure leads to smoothing and reduction of the variability of neutron intensity. This damped intensity gives a better reproduction of the conditions on the orchard. Consistent irrigation and stable climatical conditions should keep the long-time soil moisture conditions relatively stable.

The soil water balance reveals a deep percolation of 30 % from the water inputs on the orchard. Thus irrigation on the present orchard has an active contribution to the artificial increase of the groundwater table. The usage of the mentioned techniques on field scale leads to a higher accuracy in the quantification of deep percolation.

A controlled irrigation management can contribute to irrigation recharge and thus can have a leading role for orchards in the affected region. By a collective water discharge to the groundwater, a general rising of the groundwater can be reached and water problems in this region of Morocco can be approached. A sustainable agricultural water management may lead to an increase in efficiency in water use and to an increase in groundwater recharge.



---

## Zusammenfassung

In der Region um Marrakesch (Marokko) haben ressourcenintensive Landwirtschaft, luxusorientierter Tourismus und raumgreifende Urbanisierung in den letzten 50 Jahren zu einer dramatischen Absenkung des Grundwasserspiegels geführt. Bei gegebenen klimatischen Bedingungen und anhaltender anthropogener Übernutzung sind die Möglichkeiten natürlicher Grundwasserneubildung stark eingeschränkt. Ein nachhaltiges Wassermanagement in der Landwirtschaft kann auf der einen Seite zur effizienteren Nutzung der Wasserressourcen beitragen und auf der anderen Seite den gezielten Beitrag zur Grundwasserneubildung regeln.

Für eine 50 ha große Mandarinenplantage, 30 km südwestlich von Marrakesch (Marokko), wurde die Grundwasserneubildung aus überschüssiger Tröpfchenbewässerung quantifiziert. Zu diesem Zweck ist eine Bodenwasserbilanz für eine Bewirtschaftungsperiode von Juni bis Dezember 2013 aufgestellt worden. Durch die Kombination der Eddy-Kovarianz-Technik (ECT) und des Cosmic-Ray-Sensings (CRS) konnte diese Bilanz auf Feldskala berechnet werden. Die ECT wurde dazu genutzt, um die aktuelle Evapotranspiration zeitlich hoch aufgelöst zu bestimmen. CRS dient zur Quantifizierung der Bodenfeuchte aus der Beziehung zwischen kosmischen Neutronenflüssen und im Boden gespeichertem Wasser. Dabei liegt der Fokus insbesondere auf der Erprobung des CRS auf heterogener Bewässerungslandwirtschaft. Aufgrund inhomogener Bodenfeuchten durch linear angeordnete Baumreihen mit Tröpfchenbewässerung, wurde eine angepasste Kalibrierung entwickelt. Diese berücksichtigt die vertikalen und horizontalen Unregelmäßigkeiten in der Errechnung des Integrals der Bodenfeuchte. Vergleichende Messungen wurden mit einem TDR, Evaporimeter und Fluxmeter zur Validierung der ECT und CRS Messungen vorgenommen. Die Anpassung der Kalibrierung an die gegebenen Verhältnisse ergibt eine generelle Reduktion und eine geringere Fluktuation der Neutronenintensität. Aufgrund klimatisch stabiler Verhältnisse und einer nahezu gleichmäßigen Bewässerung bildet die gewichtete Bodenfeuchte die Verhältnisse auf der Plantage deutlich besser ab.

Die Berechnung der Bodenwasserbilanz zeigt, dass 30 % der aufgebrachten Bewässerung und des eingegangenen Niederschlages als Grundwasserneubildung im Boden versickern. Somit trägt die Mandarinenplantage aktiv zur Erhöhung des Grundwasserspiegels in der Region bei. Die Verwendung der zwei feldmaßstäblichen Technologien führt zu einer höheren Genauigkeit in der Errechnung der Bodenwasserbilanz und zu der Erkenntnis, dass die Kombination dieser beiden Techniken durchaus sinnvoll unter gegebenen Bedingungen ist.

Die künstliche Grundwasserneubildung durch Bewässerungsüberschuss kann mit diesen Ergebnissen auch auf andere Plantagen und landwirtschaftliche Betriebe übertragen werden. Durch gemeinschaftlichen Wassereintrag durch oberflächlich geliefertes Bewässerungswasser kann somit sukzessive eine Erhöhung des Grundwasserspiegels erreicht und die Wasserknappheit in betroffenen Gebieten eingedämmt werden.



# Contents

<b>Abstract</b>	I
<b>Zusammenfassung</b>	III
<b>List of Figures</b>	VII
<b>List of Tables</b>	IX
<b>Nomenclature</b>	XI
<b>1 Introduction</b>	1
<b>2 Study Area</b>	5
2.1 Geography . . . . .	5
2.2 Climatology . . . . .	6
2.3 Geology . . . . .	7
2.4 Hydrology and Water Resources . . . . .	7
<b>3 Methodology</b>	9
3.1 Soil Water Balance and Groundwater Recharge . . . . .	9
3.2 Eddy Covariance Technique . . . . .	13
3.2.1 Methodological Principles . . . . .	13
3.2.2 Measurement Setup . . . . .	14
3.2.3 Horizontal and vertical Extension of the Measurement Size . . . . .	15
3.2.4 Flux Calculation and Correction . . . . .	15
3.3 Cosmic Ray Neutron Sensing . . . . .	16
3.3.1 Production of Cosmic Rays and their Interactions in Soils . . . . .	17
3.3.2 Horizontal and vertical Extension of the Measurement Size . . . . .	19
3.3.3 Correction of Neutron Intensity and Calibration of the Probe . . . . .	21
3.4 Water Management Modeling . . . . .	24
<b>4 Experimental Site and Field Activities</b>	29
4.1 Experimental Site . . . . .	29
4.2 Soil Water Balance . . . . .	30

## *Contents*

---

4.3 Eddy Covariance Technique . . . . .	31
4.4 Cosmic Ray Probe . . . . .	32
4.4.1 Correction of the Neutron Intensity . . . . .	32
4.4.2 Calibration of the CRP . . . . .	33
<b>5 Results</b>	<b>39</b>
5.1 Cosmic Ray Neutron Counts and Calibration . . . . .	39
5.1.1 Calibration . . . . .	40
5.1.2 Texture Analysis . . . . .	44
5.2 Soil Water Balance . . . . .	45
5.2.1 Precipitation and Irrigation . . . . .	45
5.2.2 Evapotranspiration . . . . .	45
5.2.3 Soil Moisture . . . . .	47
5.2.4 Bottom Flux . . . . .	52
5.3 Water Management Modeling . . . . .	56
<b>6 Discussion</b>	<b>61</b>
6.1 Assessment of Irrigation Recharge . . . . .	61
6.2 Applicability of CRS on heterogeneous Soil Conditions . . . . .	62
6.3 Soil Water Balance on Field Scale . . . . .	64
6.4 Outlook . . . . .	65
<b>Conclusion</b>	<b>69</b>
<b>Appendix</b>	<b>VII</b>
Appendix I . . . . .	VII
Appendix II . . . . .	VIII
Appendix III . . . . .	VIII
Appendix IV . . . . .	IX
<b>Declaration of Academic Honesty</b>	<b>XI</b>

# List of Figures

2.1	Hydrology and groundwater depletion of the Haouz plain . . . . .	5
2.2	Climate graph of Marrakesh . . . . .	6
3.1	Soil water balance of an exemplary cropped field . . . . .	10
3.2	Principles of the eddy covariance technique . . . . .	13
3.3	Contribution of the partial flux measured by the eddy covariance technique . . . . .	15
3.4	Cascade reaction of primary cosmic rays in the atmosphere . . . . .	18
3.5	Calculation of the water stress coefficient . . . . .	26
4.1	Pattern of linear trees lines with irrigation and locations of the sampling strategies	30
4.2	Energy closure of the eddy covariance measurements . . . . .	31
4.3	CRP and ECT installed on a tower on the orchard . . . . .	32
4.4	Size of the footprint of the CRP and sampling pattern of campaign one . . . . .	34
5.1	Raw and corrected neutron counts per hour . . . . .	39
5.2	Box-plots of the three correction factors . . . . .	40
5.3	Soil moisture for plots I - IV measured with the FDR . . . . .	41
5.4	Results of the soil moisture sampling campaigns one and two . . . . .	43
5.5	Relation between evapotranspiration, irrigation and precipitation . . . . .	46
5.6	Soil moisture measured by TDR and by CRS . . . . .	47
5.7	Mean variation of the soil moisture aggregated for the hours of the day, measured by the CRP . . . . .	48
5.8	Soil moisture in different depths of the TDR . . . . .	49
5.9	Mean variation of the soil moisture aggregated for the hours of the day, measured by the TDR. . . . .	50
5.10	Relationship between soil moisture and actual evapotranspiration . . . . .	52
5.11	Bottom flux, calculated by the SWB with two options of soil moisture storage change . . . . .	53
5.12	Bottom flux calculated with actual and reference evapotranspiration . . . . .	54
5.13	Comparison of modelled and calculated values of <i>SM</i> , <i>ETa</i> and <i>DP</i> . . . . .	57



# List of Tables

5.1	Statistical summary of weighted and unweighted soil moisture . . . . .	42
5.2	Results of the texture analysis . . . . .	44
5.3	Weekly values of the components of the soil water balance . . . . .	55
5.4	Coefficient of determination for bottom flux and single components of the SWB .	56
5.5	Results of irrigation modelling from the WatBal model . . . . .	59



# Nomenclature

BF	Bottom Flux
COSMOS	COsmic ray Soil Moisture Observing System
cph	Counts Per Hour
CRP	Cosmic Ray Probe
CRS	Cosmic Ray Neutron Sensing
DP	Deep Percolation
ECT	Eddy Covariance Technique
ET0	Reference Evapotranspiration
ETa	Actual Evapotranspiration
ETc	Potential Crop Evapotranspiration
FDR	Frequency Domain Reflectometry
MCNPX	Monte Carlo N-Particle extended
SM	Soil Moisture
SOC	Soil Organic Carbon
SOM	Soil Organic Matter
SWB	Soil Water Balance
TAW	Total Available Water
TDR	Time Domain Reflectometry
TERENO	TERrestrial ENvironmental Observations



# 1 Introduction

A semi-arid to arid climate, proceeding climatic changes and an increment in water consumption behavior in the last century, lead to problems in the water supply for several parts of Morocco. Especially with introduction of the “Green Morocco Plan/Plan Maroc Vert” a new intensive agriculture was performed Lepage (2012). Thus the importance of available water got urgent. Especially in the region around Marrakesh with an increasing number of tourists, growing urbanization and an intensive agricultural usage. Being one of the most important touristic spots in Morocco, Marrakesh has undergone a dramatic change in growth and size. In the last decade, the city was subject to a substantial increase in urban structures: big hotels and cheap flats (for an arising middle class) were built and many golf courses emerged on dry savanna soil around the city (Lepage, 2012). With a steadily increased gross domestic product from 37 bn to 99 bn US Dollar in the last decade, the living standard for a remarkable part of the population also increased (Wirtschaftskammer Österreich, 2013). As a result the water consumption rose inevitably. While industrial and civil water consumption adds up to 20 %, agriculture is the main consumer of Moroccan water resources (80 % of total consumption) (United Nations Environment Programme, 2008). Citrus, olives and cereals are mainly produced in the warm and sunny regions and need a high amount of water under local conditions. Until 2002 more than 90 % of the economically active population was employed in agriculture with only a small contribution to the gross domestic product (United Nations Environment Programme, 2008).

The water used for irrigation of fields and orchards originates from wells, from surface water (transported by mostly artificial systems across the country) and from ancient subsurface channel systems (coming from the High Atlas). Overexploitation results from more than 24000 private and illegal wells which draw around  $6.5 - 7 * 10^8 \frac{m^3}{y}$  groundwater for irrigation<sup>1</sup>. Due to heavy overconsumption as well as high vulnerability to climatic hazards like droughts, the observed region shows a groundwater depletion of more than 40 meters in the last 35 years (Lepage, 2012). Additional water resources like the ancient subsurface channels were dried-up because of heavy groundwater depletion. Due to deforestation, inappropriate cultivation practices and thus implied soil erosion in the High Atlas, the barrages were silted up and now only a notably smaller amount of water can be stored for the supply of the plains (United Nations Environment Programme, 2008).

---

<sup>1</sup>Workshop notes from the Kick-off workshop on 19.03.2013 in Marrakesh

Because of the mentioned problems, a better water management is needed to provide sufficient water resources in all regions. This aim could be reached by a lower water consumption of all stakeholders or a secured water supply. Not only better irrigation systems like surface and subsurface dripper, micro sprinkler and spray irrigation and their dimensioning can contribute to this goal. The raise of the regional groundwater table is another important factor for irrigation water delivery.

One indicator of the current inconvenient water- and irrigation management is the continuous lowering of the groundwater table. To improve the irrigation management, a detailed look on the effects of the current practices is necessary. A soil water balance can be used to determine and quantify the bottom flux ( $BF$ ) from the root-soil system and thus the effective groundwater recharge through irrigation. A study area near Marrakesh was selected to assess irrigation management and the interaction with the groundwater table. The investigated area is a 13 year old citrus orchard west of Marrakesh with a sectoral installed surface drip irrigation system.

The main components of the soil water balance on the specific area consist of irrigation and precipitation as inputs and evapotranspiration and the storage changes in soil water content. The input can be measured directly by a water meter and a rain gauge. Evapotranspiration is measured by the eddy covariance technique which quantifies the transport of latent heat by turbulent movements of the air. By this technique different matters in the atmosphere (e.g., water vapor, latent heat,  $\text{CO}_2$ ,  $\text{CH}_4$ ) can be quantified. They are moving due the influence of wind, heat convection or saturation deficits. Those movements, called eddies, are measured by very sensible devices with a high detection frequency.

For the measurement of the soil moisture ( $SM$ ) there exist several measurement techniques on different spatial scales. On point-scale geoelectrical and geophysical techniques are available. On field-scale just few methods like cosmic ray sensing or gravity measurements are well developed. Whereas on large spatial scale remote sensing is common but gives only poor-resolute soil moisture information (Vereecken et al., 2013). In the present study cosmic ray sensing was applied (CRS). A cosmic ray neutron probe (CRP) was constructed in the middle of the orchard. With a footprint of nearly 300 m in radius, this technology can quantify the soil water content on an inverse correlation to the measured neutron intensity. Neutrons are generated by cascade reactions both in the atmosphere and soil and are moderated or stopped by hydrogen in the environment. According to the backscattered neutron intensity from soil, its water content can be derived. This technology was developed by working group of the University of Arizona and implemented in the COsmic ray Soil Moisture Observing System (COSMOS) in the United States of America, which is a measuring network of more than 50 cosmic ray neutron sensing probes distributed all over the country (Zreda et al., 2012). Former studies investigated the applicability of the technology in various places: on a coastal site on Hawaii (Desilets et al., 2010), on an area in the desert of Arizona (Franz et al., 2012a), on a snow site in the high mountain range in Arizona

(Desilets et al., 2010), in a humid forested ecosystem in Germany (Bogena et al., 2013) and on an agricultural site with different stages of crop growing in Germany (Rivera Villarreyes et al., 2011). In these studies, the applicability of the technology for quite homogenous soil moisture conditions in the footprint is well prospected.

The present study focuses on heterogeneous soil and vegetative conditions and creates new challenges on the application of the method. The uneven distribution of linear wet tree lines and dry ways made the development of a modified calibration methodology necessary. For this purpose, two soil sampling campaigns were conducted to receive a better impression of the soil moisture conditions in the field. The first was realized in the recommended sampling scheme (Zreda et al., 2012) and the second in a modified scheme, which considers the areas with different soil moisture conditions. After calculating soil moisture from detected neutron intensity, a soil water balance was derived on a daily basis and solved for the bottom flux.

According to the preceding issues, the following research questions can be stated for the investigations:

- Is the diurnal dimensioning of irrigation water amount appropriate? Is there excess irrigation water which contributes to the groundwater recharge?
- Is the cosmic ray neutron sensing usable with a high temporal resolution in irrigated, semi-arid regions? Are improvements for calibration needed?
- Are the eddy covariance technology and cosmic ray neutron sensing combinable for calculating a soil water balance on field scale?

This thesis is part of the project "River runoff from headwater catchments transformed to groundwater recharge in the Haouz plain, Upper Tensift basin (Morocco)" funded by the German Federal Ministry of Education and Research - BMBF. Participants are the University of Potsdam, the University Cady Ayyad Marrakesh and the laboratoire mixte international "Télédétection et Ressources en Eau en Méditerranée semi-Aride" (LMI TREMA). The coordinators of the project are Prof. Lahoucine Hanich (University of Marrakesh) and Dr. Till Franke (University of Potsdam). With this thesis, the knowledge about the applicability of cosmic ray neutron sensing under mentioned conditions is supposed to be improved and its usefulness in irrigation practice should be assessed.



## 2 Study Area

### 2.1 Geography

The present study was conducted on a citrus orchard 30 km southwest of Marrakesh, Morocco. The orchard is situated near the small village Ait Cheikh and belongs to the administrative province Al Haouz in the region Marrakesh-Tensift-El Haouz, which has a size of 31.160 km<sup>2</sup> and a population of 3.1 mil inhabitants (Royaume du Maroc, 2005).

The Haouz plain covers an area of 6.000 km<sup>2</sup> and is part of the larger Tensift basin, which is named after the river Oued Tensift. In the north it is bounded by the Jbellet massif and in the south and east by the Marrakesh High Atlas, while the western boundary is the Atlantic Ocean. Figure 2.1 shows the area of the Haouz plain, its aquifer and hydrological situation (explained in section 2.4). The region around the orchard is a rural, sparsely populated land with mainly pasture farming and irrigated citrus and olive orchards.

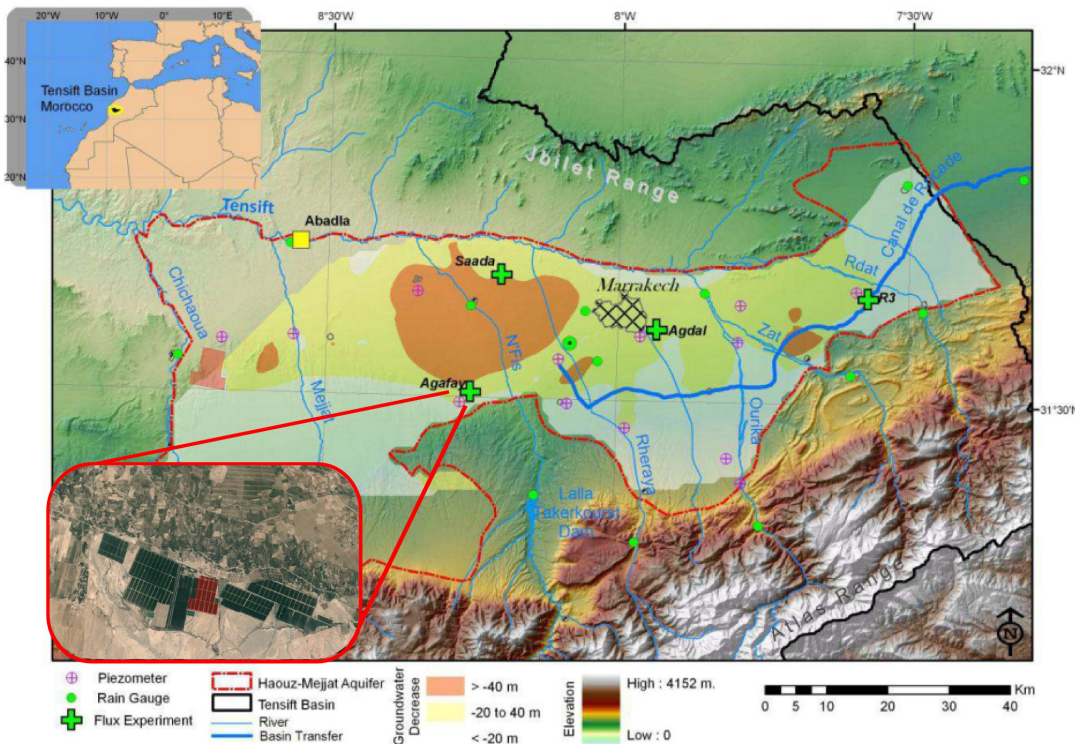


Figure 2.1: Geography and hydrology of the Haouz plain. The examined citrus orchard near Agafay is enlarged. The red-shaded area is the study area within the CRS footprint (modified after Lepage (2012)).

## 2.2 Climatology

Located in the northwestern part of the African continent, Morocco is influenced by the Atlantic Ocean, the High Atlas and the Sahara desert. Due to these impacts, the country possesses different climate gradients. The northern part of the country is characterized by the Mediterranean climate with rainy, mild winters and hot summers. With lower latitudes, the amount of rain decreases and the mean annual temperature increases. The country thus encounters an intense north-south gradient with increasing aridity and decreasing precipitation. An intense west-east gradient from maritime to continental climate exists with increasing seasonality in temperature and decreasing precipitation.

The investigated area is located between the Atlantic Ocean and the High Atlas and mainly influenced by continental climate. Following the classification of Köppen-Geiger, the region around Marrakesh is of the type Bsh<sup>1</sup>. The mean annual temperature is 19.6 °C and the average annual precipitation 345 mm (figure 2.2).

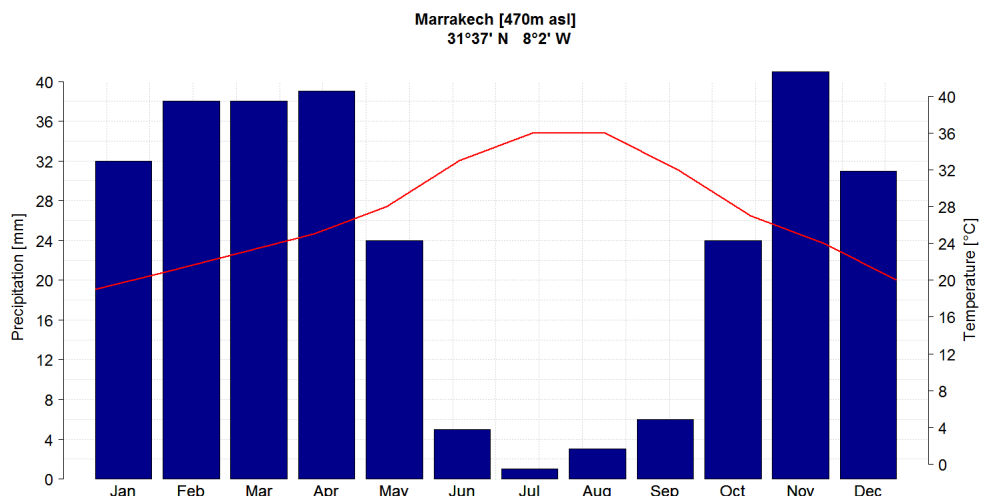


Figure 2.2: Climate graph of Marrakesh. (Data Source: Deutscher Wetterdienst (2013))

Due to high temperatures and low relative humidity, most of the precipitation and irrigation returns as evapotranspiration to the atmosphere. The annual average evapotranspiration of 1380 mm is a feature of the water-limited, climatic conditions (Er-Raki et al., 2012). The precipitation has a high intra and inter annual variability due to unpredictable torrential downpours, which are typical for dry savannas. The occurrence of such events showed a decreasing trend in the last century (United Nations Environment Programme, 2008).

<sup>1</sup>Bsh stands for a semi-arid climate or steppe climate: hot and dry summers and mild and wet winters.

## 2.3 Geology

Morocco is located at a special geological triple junction, consisting of a continent (Africa), an ocean (Atlantic Ocean) and an active plate collision zone (African and Eurasian plates) (Michard, 2008). The country thus has a broad variety of geological and morphological forms, which influence landscape and climatology. The four large mountain ranges: Rif, Middle-, High- and Anti Atlas are of different types of formations and arose from two important origination processes that occurred on the territory of Morocco: in the Precambrian and Paleozoic (300 My ago) the geological basement of the southern part of the country, the High Atlas including the Anti-Atlas and parts of the High- and Middle Atlas, originated by a collision of continents. In contrast, the north of the country was generated by the Alpidic orogeny in the Tertiary (65 My ago) when the African and Eurasian plate collided and as a result the Rif was formed.

The High Atlas reaches a height of 4.167 m (Djebel Toubkal) and is based on crystalline stones. Apart from that is covered by Mesozoic sediments in the middle and east. Wide plains in front of these mountain ranges are characterized by typical alluvial deposits from the High Atlas which were transported by heavy rain events and snow melt (Michard, 2008). The Haouz plain as a piedmont is characterized by Mesozoic sediments as well by Neogene molasses and alluvial deposits (Michard, 2008).

## 2.4 Hydrology and Water Resources

Due to Morocco's location in the semi-arid climate zone, water is a very critical and important resource for the agriculture and the population. About 85 % of available water is used for irrigation, which makes a good supply management important (Amenzou et al., 2013). The observed watershed is the Tensift basin, located in the Haouz plain. Since 1995, Moroccan water management is regulated by the "Water Law". It allocates the water management into decentralized water agencies. For the considered area the Agence du Bassin Hydraulique du Tensift is responsible for the planning, protection and conservation of the water resources in the Tensift basin (Lepage, 2012).

The examined orchard is located in the Tensift basin and its main river, the Tensift, flows from the High Atlas Mountains to the Atlantic Sea, passing Marrakesh in the north. The High Atlas functions as one of the main water resources for the central region of the country. The water, generated by snow melt and precipitation, flows in smaller rivers through the Haouz plain and drains into the Tensift. High fluctuations of drainage are induced by intensive runoff events and high temperatures, which poses irrigation problems (Müller-Hohenstein and Popp, 1990). Episodic discharges in rivers can reach a high volume and velocity and thus transport vast amounts of sediment.

Due to its aridity and lacking water resources, freshwater has to be delivered to the urban and

agricultural structures in the plain. In ancient times, the water supply of the Haouz plain was secured by 'khettaras' or 'séguias' which are excavated underground aqueducts that transport water from the mountains to agricultural areas in the plain<sup>2</sup> (Lepage, 2012). This transport technique was mostly abandoned in the beginning of the 20th century due to lowering of the groundwater table at the source of the 'khettaras' caused by overconsumption. Hence, there was a lack of the gradient to ensure water flow to the plain. The traditional transport technique was replaced by electrical pumping of groundwater. At that time, reservoirs were built in the mountains to provide drinking and irrigation water supply in the plain. Additionally, those reservoirs were built to cut peak flows and thus made settlement close to the river more secure. The water from the reservoirs is transported to the plain by smaller rivers or by artificial channels as the 'Canal de Rocade' (figure 2.1) (Lepage, 2012). The annual amount of water, used in the Tensift basin is around  $1.45 \times 10^{12} \text{ m}^3$ . It is delivered by 28 % groundwater, 54 % by the reservoir Lalla Takerkoust and a bit by traditional 'khettaras' and 22 % by water transfer from the Oum Er-rbia basin (Limam, unknown).

Once groundwater was one of the most important water resources for the plain. However, as a consequence of the intensive usage of groundwater due to the increasing population and agricultural production in the 20th century, the groundwater table was lowered drastically. The inflow to the unconfined aquifers of the Tensift basin (the Haouz, Mejjate, and Bahira aquifer) which consist of very heterogeneous alluvial deposits is fed from the High Atlas (United Nations Environment Programme, 2008). The thickness of the aquifer is very variable: from 120 m in the southern area, where the abstraction is smaller because of a lower consumption and the spatial proximity to the mountains, to 20 m in the northern area, where Marrakesh and its agriculture have a high water consumption (United Nations Environment Programme, 2008). As shown before in figure 2.1 the biggest depletion occurs west of Marrakesh, near the studied area. In this part large areas of irrigated agriculture exist and cause an annual depletion of the groundwater table of around one to three meter (Lepage, 2012). Aquifer recharge only occurs near bigger rivers (influential conditions) or by groundwater fluxes from recharge areas (e.g., High Atlas)<sup>3</sup>.

---

<sup>2</sup>Ancient system for water distribution in arid lands and deserts, located near mountains. Due to the higher groundwater levels in the mountains, the water was easily transported by a slight slope to the plains by gravity (Lepage, 2012).

<sup>3</sup>Workshop notes from the Kick-off workshop on 19.03.2013 in Marrakesh

# 3 Methodology

## 3.1 Soil Water Balance and Groundwater Recharge

The mentioned groundwater depletion in the region around Marrakesh makes a better water management necessary. Especially in irrigated agriculture, high amounts of ground and surface water are used. To assess irrigation effectiveness and improve water management, a soil water balance (SWB) was measured for the considered citrus orchard on field-scale.

The availability of water in plant-soil-systems determines the conditions and limitations of growth and should be kept stable by irrigation. After Hillel (1998) the field water balance is defined as “[...] an account of all quantities of water added to, subtracted from and stored within a given volume of soil during a specified period of time.”

Under arid conditions, careful management of agricultural used water is an essential point at the intersection of yield and environmental issues. Insufficient irrigation induces wilting and loss of plants, while watering that exceeds the vegetative demand may drown the plant, drain as runoff or evaporate from the soil.

To have a tool for quantification of irrigation practice effectiveness, the soil water balance can be calculated and solved for groundwater recharge. It provides an insight to the amount of water, percolating unused through the root zone to the aquifer. The components of the balance are shown in figure 3.1 and in equation 3.1:

$$0 = P + I - A - ET_a \pm \Delta S - DP \quad (3.1)$$

$P$	precipitation	$[\frac{mm}{d}]$
$I$	irrigation	$[\frac{mm}{d}]$
$A$	runoff and subsurface flow	$[\frac{mm}{d}]$
$ET_a$	actual evapotranspiration	$[\frac{mm}{d}]$
$\Delta S$	changes in soil water content	$[\frac{mm}{d}]$
$DP$	deep percolation/groundwater recharge	$[\frac{mm}{d}]$

The determination of the components takes place on different spatial and temporal scales. Over the last decades, the accuracy of the measurements increased due to technical progress and improved storage media. Some of the most important methods and devices are introduced below.

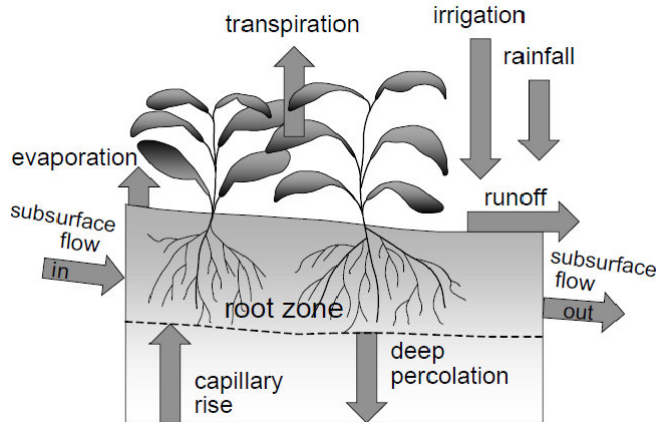


Figure 3.1: Comprmts of a soil water balance of an exemplary cropped field. (Allen, 1998)

**Precipitation** is measured by different types of rain gauges: the standard Hellmann type, the tipping bucket rain gauge and the weighing rain gauge. All measurements are on point scale and combinable with a data logger, yielding a high temporal data resolution (See Dyck and Peschke (1983) for more information).

**Irrigation** can be measured directly by referring the pumping rate to the irrigated area or by having a water meter at the outlet of the pumping station.

In the specific flat area as in the present study, **lateral flow** like runoff and subsurface flow can be neglected, thus quantification methods are not conducted in the investigated scenario.

**Evapotranspiration**, consisting of soil evaporation and plant transpiration is concurrently the most complex measurement. Two types of evapotranspiration can be distinguished: potential and actual evapotranspiration. The potential ( $ET_c$ ) or reference evapotranspiration ( $ET_0$ ) describe the evapotranspiration from water saturated areas with not limited water supply. As defined after Allen (1998)  $ET_0$  is the evapotranspiration of the hypothetical grass reference crop with assumed crop height of 0.12 m, a fixed surface resistance of  $70 \frac{s}{m}$  and an albedo of 0.23. The actual evapotranspiration ( $ET_a$ ) describes the evapotranspiration for a given water supply in the area (Dyck and Peschke, 1983).  $ET_a$  is always lower than or equal to  $ET_0$  because it cannot exceed the available maximum water yield. Evapotranspiration mainly depends on solar radiation which is characterized by spatial and temporal variations all over the world (Hillel, 1998). For the quantification of  $ET_0$ , a Class-A-Pan or the FAO-56 Penman-Monteith equation are typically applied. Lysimeters can determine the evapotranspiration by measuring the loss of water to the atmosphere through weighing. An additional option is the calculation of the latent heat by an energy balance. The latent heat is a direct indicator for evapotranspiration

and by multiplication of a conversion factor it can be transformed to  $ET_a$ . But the result is only that exact as the single components of the balance. The eddy covariance technique (ECT) is a precise, but complex method for the calculation of  $ET_a$ . Since this technique is used in the present study, a detailed description is given in section 3.2.

Changes in the **soil water content** can be estimated by direct and indirect methods. A direct measurement is the thermogravimetric method, where soil samples are weighed before and after drying on 105°C to determine the soil moisture. Inexact results due to disturbances of the soil structure when taking soil samples and labor-intensive sampling campaigns make this measurement unhandy. For an indirect measurement, several techniques exist, for example lysimeter, hydrogeophysical methods, remote sensing and cosmic ray neutron sensing (Vereecken et al., 2013).

A lysimeter is suitable for long time measurements, but due to its high installation costs and the distorted soil conditions (no horizontal flow and disturbed soil monolith) its use is critical. Another analogous technique is the tensiometer which measures the matric suction of the soil, using the correlation of matric suction and soil moisture (the lower the soil moisture, the higher matric suction in the soil) (Dyck and Peschke, 1983). Other techniques for the quantification of changes in soil water content are geophysical point measurements like the time domain reflectometry (TDR), the frequency domain reflectometry (FDR) or capacitance sensors. These approaches measure the electrical permittivity of the soil, which is a direct indicator for the water content. They provide reproducible values of local soil moisture, mostly graduated for the depth, but just on point scale. The advantage of the latter techniques is a convenient measurement on larger time scales, due to their permanent installation in the soil. Disadvantages are high costs for the installation of distributed networks to cover a bigger area and a high effort for maintenance and processing (Hillel, 1998). Other techniques, using electrically induced pulses which give information about traveling times in the soil and thus about the permittivity are, e.g., ground-penetrating radar (using electromagnetic waves), electromagnetic induction (using induced magnetic fields in the soil), electrical resistivity tomography (using differences in electric potential induced by electrodes) or gamma ray adsorption (using cesium-emitted radiation) (Hillel (1998) and Vereecken et al. (2013)).

To obtain an integral value of soil moisture for a large area, there exist several options. One is the usage of remote sensing. Satellite missions used for this aim are the Soil Moisture and Ocean Salinity (SMOS) with a resolution of 40 km (Chehbouni et al., 2008) or the Soil Moisture Active Passive (SMAP) starting in October 2014, with the use of RADAR and radiometers. Using remote sensing, it is possible to measure the soil moisture for large areas without any limitations because of rough terrain or geopolitical restrictions. The measurement depth is, however, limited to the first centimeters in the soil, which makes it impossible to make assumptions of the soil moisture dynamics in deeper layers. Due to high costs and varying repeating times of coverage,

the temporal resolution is often too low to obtain detailed information of the dynamics in the soil (Franz et al., 2012b). A second option is the usage of the gravity field of the earth. By measuring differences in gravity, which are a direct indicator for mass changes, water content changes on the earth can be determined. By additional measurements of single components of the hydrological cycle, the soil moisture can be determined. However, this satellite-based measurement is on a large temporal and areal scale and does not give high-resolut soil moisture information on field-scale (Güntner et al., 2012). An often used option is a distributed sensor network, where several soil moisture sensors of one kind are combined to a certain sampling pattern, installed in the soil. They give dependent to the accuracy of installation, a realistic reproduction of heterogeneous conditions in the field. An additional option for an extensive and indirect measurement of soil moisture is cosmic ray sensing, which is described in more detail in section 3.3.

The amount of water, that does not evaporate or drain off, infiltrates to the root zone (assuming absent lateral flow) as **bottom flux** and moves towards the groundwater table as **deep percolation**. Bottom flux is the water movement in the soil-root-zone. It can be upwards or downwards directed. If it is not taken up by roots it percolates downward through the vadose zone to the groundwater. The amount of water percolated depends on the amount of available water (precipitation, irrigation) and the hydraulically characteristics of the soil. These soil properties<sup>1</sup> can vary on small scales due to their dependence on soil texture, soil structure (roots, macropores) and water content. Bottom flux (*BF*) or deep percolation (*DP*) represent the groundwater recharge and can be quantified by the indirect method of a SWB. Its reliability depends on the precision with which the measurement of the remaining components of the SWB can be determined. A direct measurement of the *BF* is also possible using the fluxmeter which works like a small subsurface lysimeter. However, the fluxmeter measurements lead to underestimations of the *BF* because it only measures a flux if the soil is saturated. Such conditions are scarce in arid regions and thus a fluxmeter should be utilized with care. As recommended by Evett et al. (1993), the direct calculation of the *BF* is possible when a fixed percentage from the precipitation is subtracted since  $ET_a$  is neglectable during heavy rainfall. However, this approach contains several uncertainties and needs a high temporal resolution of the precipitation data.

Tracers are also well developed tools for quantification of BF. Stable isotopes ( $^{18}O, ^{16}O$ ), salt tracers (e.g., Sodium chloride, Potassium chloride, Bromide, Lithium), radioactive substances (e.g.,  $^3He, ^{51}Cr, ^{114}In$ ) and nonfluorescent dyes (e.g., brilliant blue) are commonly used tracers (for more details see Leibundgut et al. (2009) and Glendon and Hillel (1988)).

In the following sections, a detailed description of the ECT and CRS, used for the computation of the SWB on field scale, is given.

---

<sup>1</sup>Particularly field capacity, hydraulic conductivity or water potential.

## 3.2 Eddy Covariance Technique

The precise determination of the actual evapotranspiration is an essential need for the calculation of a SWB. The aforementioned approaches are time-consuming, expensive or built on assumptions. The development of the ECT made a determination of  $ET_a$  much easier and more precise. The ECT, developed in the 1980s, is a micrometeorological technique for the measurement of different turbulent energy and matter fluxes, e.g., latent heat, water vapor, carbon dioxide, methane or other trace gases.

### 3.2.1 Methodological Principles

Water vapor or different gases in the atmosphere are in a ceaseless movement, induced by wind, heat convection or saturation deficits. These movements occur as eddies, which rotate from the source of the matter into the free air or to a deficit of the matter. The direction of rotation depends on the concentration gradient of the substance in the air or the temperature of the parcel. Water for example evaporates from the moist surfaces and arises into the air (figure 3.2). These fluctuations lead to eddies with different velocities and diameters. Their size depends on surface roughness, wind speed and height above the surface (Huang et al., 2011).

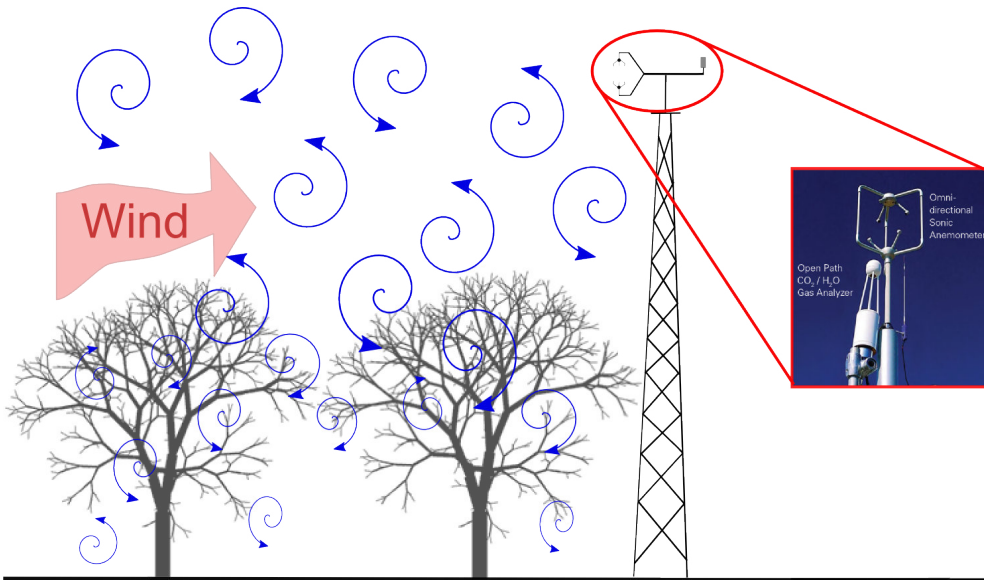


Figure 3.2: Principles of the eddy covariance technique: rotating eddies are measured by an anemometer and a gas analyzer, installed on a tower in the middle of the observed area. The sonic anemometer and the gas analyzer are enlarged to show detailed set up (modified after Burba (2013)).

The higher and rougher the area, the bigger the eddies and the slower their frequency and their rotation velocity (Burba, 2013).

The mathematical basis for the calculation of turbulent fluxes is given by the Reynolds decomposition, which is based on the calculation of the covariance between wind speed and gas concentration (Huang et al., 2011). The flux ( $F$ ) at each time step is calculated by using air

density, vertical wind speed and the dry mole fraction of water vapor. These terms are decomposed to a time series with a time-mean ( $\bar{x}$ ) and time-fluctuating part ( $x'$ ) (deviations from these time-means) (Burba, 2013):

$$F = (\overline{\rho_d \bar{w}' s'}) \quad (3.2)$$

$\rho_d$	air density	$\left[ \frac{kg}{m^3} \right]$
$\bar{w}'$	time mean and time fluctuating part of vertical wind speed	$\left[ \frac{m}{s} \right]$
$\bar{s}'$	time mean and time fluctuating part gas concentration	[ppm]

### 3.2.2 Measurement Setup

Usually ECT systems are installed on a tower which is situated in the middle of the observed area and at a height twice of the canopy (Foken, 2006). The station consists of a temporally high-resolute sonic anemometer and a gas analyzer (figure 3.2). Additional meteorological information are needed for the correction of the data. For this aim, devices for the measurement of temperature, soil heat flux and solar radiation are commonly installed (Burba, 2013).

The **sonic anemometer** measures three-dimensional wind speed by signal travel times and distances between the signal generators. To account for high fluctuations in wind components, the device has a very high measurement frequency<sup>2</sup> (Foken, 2006).

Concentrations of CO<sub>2</sub> and water vapor are recorded by an **optical gas analyzer** which determines the intensity of optical signals as a proxy for the concentration of the observed gas. The optical signal is weakened and scattered by gas molecules in the sampling volume (Burba, 2013). Two systems exist for the quantification of gas concentrations: open- or closed-path systems. They differ in the location of detection: in an open-path system the gas is analyzed in the free air, whereas in a closed-path system the gas enters a defined sampling cell.

The sonic anemometer and the gas analyzer are commonly installed closely together, to avoid fluctuations based on spatial differences. For the installation of the probe it is important that the station design does not influence or disturb the measurement of the flux. For this aim, the devices have to be mounted with an appropriate distance from the tower (Foken, 2006). The installation of the devices following the main wind direction is another important factor to avoid a tailback in the upstream flow or artificial turbulences at the devices (Aubinet et al., 2012). Since the ECT does not work during heavy rain events, data gaps can occur and have to be interpolated afterwards (Burba, 2013).

---

<sup>2</sup>The frequency usually ranges between 10 - 20 Hz, which stands for a detection interval of 10 - 20 counts per second.

### 3.2.3 Horizontal and vertical Extension of the Measurement Size

The area upwind, where the main flux originates from, is called footprint. It is a rather variable area and depends on several factors affected by local and meteorological conditions. The main fraction of the flux neither comes from the area directly underneath the tower, nor from very large distances, but from somewhere in between (Burba, 2013).

The size of the footprint mainly depends on four factors: surface roughness, measurement height, wind direction and thermal stability. Rough surfaces like trees, houses or high vegetation disturb the eddy rotations. With increasing roughness of the surface, the size of the footprint decreases (Burba, 2013).

The installation height of the ECT determines the measured eddy sizes: shallow installed instruments measure high-frequent eddies (smaller sizes) while high mounted devices measure lower-frequent eddies (Aubinet et al., 2012). This relationship is shown in figure 3.3 where the portion of flux, measured in the footprint, and the distance from the tower are plotted against each other.

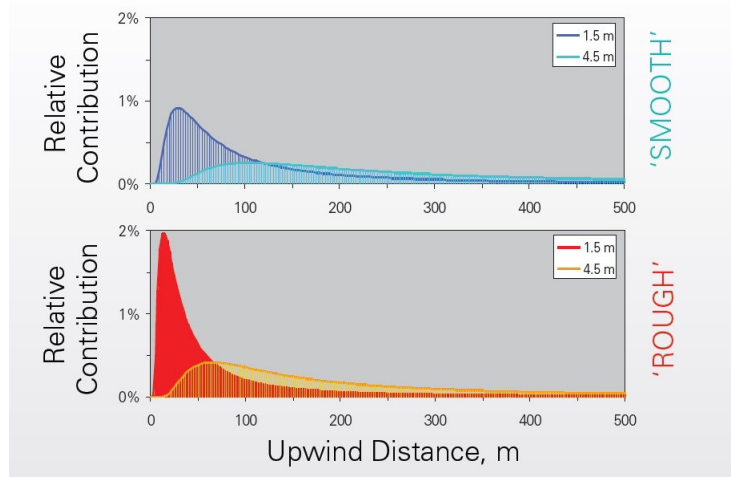


Figure 3.3: Relative contribution of partial flux to the overall flux and influence of height of the device and roughness of the surface to this parameter. (Burba, 2013)

Flux intensity is higher for locations with higher roughness and for locations closer to the tower. For both cases an increasing installation height smoothen the peak contribution of flux. At lower heights, the roughness has a bigger influence on the footprint. The ideal condition for ECT measurements is a flat terrain with a homogenous coverage which is characterized by a uniform thermal behavior and height of the canopy (Aubinet et al., 2012).

### 3.2.4 Flux Calculation and Correction

Since components of evaporative flux (wind and gas profile) are sensitive to meteorological conditions and its changes, several corrections have to be implemented in the calculation. For this aim, several software packages have been developed for the different sensors, to obviate elaborate

calculations (detailed descriptions in Burba (2013)). For the calculation of the eddy flux, first a **qualitative control** of the raw data is necessary. Spikes, dropouts, constant values, data gaps or noise in the signal have to be removed (Aubinet et al., 2012). After those revisions, the flux can be calculated by equation 3.2, using **covariance** of air density, gas concentrations and vertical wind velocities.

An important correction is the **time lag adjustment** between the signals of the gas analyzer and the sonic anemometer. Time lags occur due to a distance between the devices on the tower. Hence temporal differences in detection can occur which are induced by differing electronic settings of the devices or travelling times of the wind and gas in the detectors (Aubinet et al., 2012). Therefore, a spatial correction is conducted. The sonic anemometer is not always installed perpendicular to the actual wind direction, since it is firmly fixed and the wind direction changes. To avoid consequent cross-contamination by the two remaining wind components of this 3-D-system, **coordinate rotations** have to be performed. Due to these rotations, the mean vertical wind speed equals zero and the device is justified as origin of ordinates (Huang et al., 2011). Varying conditions in gas densities, which occur for example due to meteorological fluctuations, are corrected by the **Webb-Pearman-Leuning density correction**. Since they do not belong to the change in gas density they are removed.

Apart from these calculations, sensor specific corrections of the evaporative flux have to be done, but will not be explained here. All corrections should be done iteratively, until their influence on the flux is negligible(Aubinet et al., 2012).

### 3.3 Cosmic Ray Neutron Sensing

Another important and sensitive part of the soil water balance is the soil moisture. It governs the growth of plants and their respiration, the activity of microorganisms and the chemistry of the soil (Hillel, 1998). As mentioned before, several methods to measure the soil moisture on different scales and at different resolutions exist. A good compromise between these scales is the cosmic ray neutron sensing. With its footprint of  $\sim 30$  ha it has an intermediate measurement size and an applicability for long time measurements. In addition it has an altering measurement depth from 12 to 70 cm.

The idea of using fast neutrons for the measurement of water contents in the environment was established by several scientists (Zreda et al., 2012). Neutrons, as a part of cosmic rays, were discovered in 1912 by the Austrian physicist Viktor Hess (Schlickeiser, 2002). Investigations were done with passive subsurface probes that already used natural neutron intensity but possessed only small footprints and a high installation effort to cover larger areas (Kodama et al., 1985). Responses of these probes to the soil moisture changes were quite poor, thus the technology changed to the active approach. Those subsurface probes produced and emitted neutrons and counted the backscattered neutrons, in immediate proximity to the emitting tube (Evett

et al., 1993). Due to the production of neutrons by radioactive elements (e.g., Americium-241-beryllium) it was expensive in acquisition and its use requires an official permission. It was also dangerous to handle those probes because of their radioactive emissions. With the switch to above ground technology the technique changed back to a passive system, due to its use of galactic neutrons. Whilst previously the measurement size was tens of centimeters around the probe, the horizontal footprint increased to hundreds of square meters. Opposite to the active technology, the passive method can also determine the first vertical centimeters of the soil<sup>3</sup>.

In the late 1990s, a group from the University of Arizona developed a cosmic ray probe for the simple and non-invasive measurement of soil moisture. They established the COsmic-ray Soil Moisture Observing System, consisting of more than 50 cosmic ray probes all over the United States of America. This network is supposed to be an experimental testing of the technology in different environments and climatic zones, aiming at obtaining information about its deployability for various meteorological purposes. Up to now, detailed investigations were made for the following environments: a coastal site on Hawaii (Desilets et al., 2010), a site in the desert of Arizona (Franz et al., 2012a) and a snowy site in the high mountain range, on Mt. Lemmon, Arizona (Desilets et al., 2010). The latest development of this group was a cosmic ray sensing rover, which allows measuring soil moisture more variably and with smaller footprints.

Another working group from the Forschungszentrum Jülich tested the technology in a humid forested ecosystem in Germany (Bogena et al., 2013) in the framework of TERENO. Researchers from the University of Potsdam investigated the CRS on an agricultural site with different stages of crop growth in Germany (Rivera Villarreyes et al., 2011) and on a mountainous site in the framework of TERENO (Rivera Villarreyes, 2014).

Hitherto there are no investigations on irrigated agricultural sites in (semi-)arid environments. The presented examination thus pioneers for this kind of combination of meteorological and agricultural conditions. As recommended by Franz et al. (2013b), the attention has to be directed to a specified calibration setup for those heterogeneous hydrological settings (see section 4.4.2).

#### 3.3.1 Production of Cosmic Rays and their Interactions in Soils

Primary cosmic rays can be defined as “extraterrestrial charged particle radiation [...] consist[ing] of a flux of electrons, positrons and nucleons with kinetic energies greater than 1 keV that bombards the earth from outside” (Schlickeiser, 2002). They originate from solar activity or from other galactic reactions. They mainly consist of protons (~90 %),  $\alpha$ -particles (~9 %) and heavier nuclei (~1 %) (Bogena et al., 2013). The intensity of cosmic rays that reach the surface of the earth depends on several factors: the solar activity (negative correlation), the elevation

---

<sup>3</sup>The active probe is installed in a depth, where its footprint ends several centimeters beneath the surface. Otherwise it detects solar neutrons that bias the induced neutron intensity. Whereas the passive probe has its highest sensitivity in the upper first centimeters of the soil.

and latitude (atmospheric and geomagnetic shielding of neutrons) of the site (Zreda et al., 2008), barometric pressure and the water vapor in the atmosphere (Rosolem et al., 2013). When cosmic rays enter the atmosphere they undergo several inelastic collisions with nuclei (Desilets et al., 2010) and are weakened or converted to other energy levels.

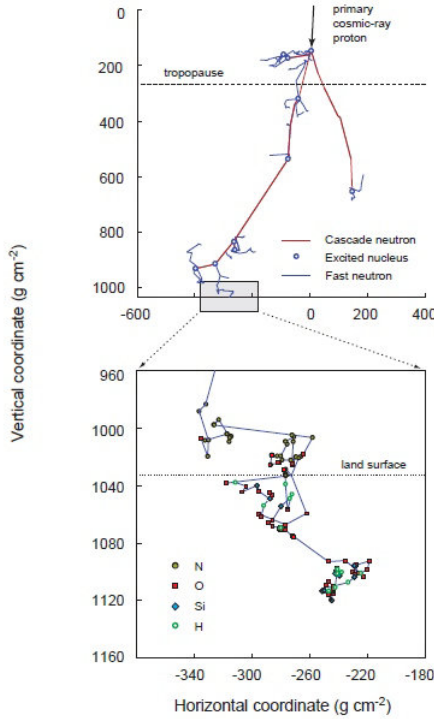


Figure 3.4: Generation of fast neutrons by cascade reaction of primary cosmic rays with different nuclei in the atmosphere and in the ground (Zreda et al., 2012).

In figure 3.4 the interaction of the particles in the atmosphere and their scattering is apparent: primary cosmic rays “collide with and disintegrate nuclei to create energetic secondary particles” (Zreda et al., 2012). When a highly energized particle enters a nucleus, it is transformed to an unstable energy level and emits a neutron to get back to a stable energy level. During this cascade reaction, neutrons of different energy levels are originated as secondary cosmic rays (Zreda et al., 2012):

- High-energy cascade neutrons [GeV] = generated by primary cosmic rays by provoking a neutron emission from a nucleus
- Fast neutrons [MeV] = emitted neutrons after a collision of high-energy neutrons and nuclei
- Thermal and epithermal neutrons [eV] = moderated neutrons that originate from collisions of fast neutrons and nuclei

In the present study observed particles are electrically neutral neutrons which have a short life span in contrast to primary cosmic rays (which are positively charged and have very long traveling distances) (Zreda et al., 2012). For CRS, fast and thermal neutrons are detected by gas-filled (mostly

$\text{He}^3$ ) aluminum detectors. In these tubes, neutrons collide with  $\text{He}^3$  and produce charged particles, which induce electronic pulses that are recorded by a detector (Baatz et al., 2014). There are two kinds of counters: a moderated one, which is shielded by polyethylene to moderate fast to epithermal neutrons, or a bare counter which consists of an unshielded aluminum detector to measure the thermal neutrons. Fast neutrons are scattered back from environmental components and are an indicator for the contained water contents. While thermal neutrons are measured to estimate the water bound in snow, vegetation, canopy water etc. (Zreda et al., 2012). Moderation of thermal neutrons is more depended on soil chemistry and thus to the macroscopic cross-section of the moderating material. Furthermore they are less sensitive to changes in soil moisture than fast and epithermal neutrons (Zreda et al., 2008). Around 40 % of the flux, measured by the neutron probe, originates from backscattered fast neutrons (Kodama et al., 1985).

As mentioned before, high-energy cascade neutrons, coming from the atmosphere, reach the soil or the surface and are moderated by hydrogen atoms. The intensity of neutron moderation depends on the characteristics of the soil and its elemental structure (Zreda et al., 2012):

- Microscopic scattering cross-sections of the occurring elements
- Energy loss by collision/number of collisions needed to moderate a fast neutron
- Abundance of elements in the environment

Hydrogen possesses best moderating power for neutrons because the lowest number of collisions is needed to thermalize fast neutrons<sup>4</sup> and is abundantly existent in the atmosphere. Opposite to rare elements which have a high moderation power as well, but that do not occur ubiquitous in the environment. Moderated neutrons are scattered back diffusively in all directions. The intensity of backscattered neutrons is higher over dry soil because only a small amount of neutrons is moderated and vice versa. This relationship between soil moisture and backscattered neutrons is used to determine the amount of water bound in the environment. Furthermore, the intensity of counted neutrons depends on the altitude of the site, the water pools in the landscape and the incoming neutrons. The intensity of backscattered neutrons also has an influence on measurement accuracy: the higher the neutron intensity, the smaller the measurement uncertainty of the technology (Shuttleworth et al., 2013).

#### 3.3.2 Horizontal and vertical Extension of the Measurement Size

A major advantage of cosmic ray sensing is its spatial extent: it covers a larger area than point measurements, but its resolution is finer than for remote sensing. The extent of the footprint, can be distinguished in two plains: horizontal and vertical.

---

<sup>4</sup>Hydrogen only needs 18 collisions to thermalize a neutron whereas most other elements need a much higher value. e.g., boron 103, carbon 113 and oxygen 149 collisions.

The horizontal extent of the footprint is “the area around the probe from which 86 % of counted neutrons arise” and in general around 600 m in diameter (Zreda et al., 2012). The mean size of the footprint was found by a Monte Carlo N-Particle extended (MCNPX) modeling, which simulates the neutron transport and distribution in the atmosphere. The spatial size of the footprint varies with altitude and atmospheric water vapor content. With increasing elevation the density of air decreases (hence the scattering mean free path) and thus the footprint increases. With decreasing water vapor content in the air the footprint increases since the neutrons undergo less collisions in the air (Zreda et al., 2012).

In contrary to a large horizontal extent, the vertical penetration depth is quite shallow: usual measurement depth varies between surface and 0.12m to 0.76m, depending on the soil moisture content (Zreda et al., 2008). In wet soils the measurement depth is shallow and limited to the upper layers where it undergoes a strong moderation of neutrons. In dry soils opposed relations occur. The penetration depth ( $z^*$ ) , given in centimeter, is defined as the cumulative depth where 86 % of the neutrons originate from and is calculated from the water bound in the soil, the organic carbon and the lattice water (after Franz et al. (2013a)):

$$z^* = \frac{5.8}{\frac{\rho_{BD}}{\rho_W} * \tau + SOC + \theta + 0.0829} \quad (3.3)$$

$\tau$	lattice water	$\left[ \frac{g}{g} \right]$
$SOC$	soil organic carbon	$\left[ \frac{g}{g} \right]$
$\theta$	soil moisture	$\left[ \frac{cm^3}{cm^3} \right]$
$\rho_{BD}$	bulk density of the soil	$\left[ \frac{g}{cm^3} \right]$
$\rho_W$	density of water	$\left[ \frac{g}{cm^3} \right]$

Neutrons produced in the upper soil layers have a stronger influence on the measured signal than deeper layers. Therefore Franz et al. (2012b) introduced a weighting function. The weighting factor ( $wt(z)$ ) is multiplied with the single layers of the soil profile:

$$wt(z) = a \left( 1 - \left( \frac{z}{z^*} \right)^b \right) \quad (0 \leq wt \leq z^*) \quad (3.4)$$

$a$  constant dependend on conserved weights

$z$  soil layer, from the surface to the penetration depth [cm]

$b$  factor that influences the curvature of the weighting function (here = 1)

There is another possibility of depth weighting, developed by a working group of the Forschungszentrum Jülich who used a fitted polynomial function of the relationship between the cumulative fraction of neutron counts in depth and the size of the footprint radius (Bogena et al., 2013).

The probe can be mounted on various heights, depending on the goal of measurement and the height of canopy. Limitations can be constituted by the height of the probe: its installation height should be lower than the mean-free path length of the air (after Franz et al. (2012a) usually around 30 m) and measurement should not be disturbed by shielding buildings or other large objects in the footprint (Rivera Villarreyes et al., 2011).

### 3.3.3 Correction of Neutron Intensity and Calibration of the Probe

Caused by different meteorological influences and vegetative conditions, the detected neutron intensity can be distorted by “total surface moisture” (Shuttleworth et al., 2013). Such interference factors are atmospheric pressure and relative humidity which are influenced by meteorological or vegetative changes (e.g., phenology of occurring crops or plants). The aim of the CRS is to measure solely the neutrons, scattered back from soil and not incoming solar radiation. Thus, an additional correction for solar and galactic neutrons is necessary. Preceding to the corrections for regional meteorological and galactic influences, the measured neutron intensity has to be corrected for losses and outliers (that are induced by technical inaccuracy and power cuts). To remove the aforementioned disturbances on the neutron intensity, following corrections have to be conducted.

**Quality Corrections** As a consequence of problems with the probe during the measurement, a lack of energy supply or complications during reading out of the data, the counting interval might not be of the chosen interval. Other problems can be outliers which differ more than 20 % from the previous value, which might occur due to the same problems. Neutron counts that are affected by these problems have to be removed from the data.

**Atmospheric Pressure** Atmospheric pressure has a strong influence on the measured neutron intensity and functions as an indicator for the density of air and thus for mass that is crossed by neutrons in the atmosphere. The higher the atmospheric pressure, the stronger the shielding and moderation of neutrons in the air. Short-time changes in weather and thus in atmospheric pressure make corrections necessary. The following correction factor ( $f_p$ ) normalizes the measured neutron intensity to the regional atmospheric pressure at the calibration time (Zreda et al., 2008):

$$f_p = \exp\left(\frac{P_0 - P}{L}\right) \quad (3.5)$$

$P_0$	mean atmospheric pressure at calibration time	[hPa]
$P$	atmospheric pressure at CRP	[hPa]
$L$	mass attenuation length for high-energy neutrons	$\left[\frac{g}{cm^2}\right]$

**Water Vapor** Water vapor is directly related to the neutron intensity because it shortens the scattering mean free path for neutrons (Zreda et al., 2012). Rosolem et al. (2013) showed that atmospheric water vapor influences the signal of neutron intensity by up to 12 %. The higher the amount of water vapor in the atmosphere, the smaller the neutron intensity. The correction factor for water vapor ( $f_{WV}$ ) was developed by Rosolem et al. (2013) and normalizes the neutron intensity to local conditions:

$$f_{WV} = 1 + 0.0054 * (\Delta_{\rho v 0} - \Delta_{\rho v ref}) \quad (3.6)$$

$\Delta_{\rho v 0}$	absolute humidity at the time of measurement	$\left[\frac{g}{m^3}\right]$
$\Delta_{\rho v ref}$	absolute humidity at the calibration time	$\left[\frac{g}{m^3}\right]$

**Incoming Neutrons** The intensity of the galactic primary cosmic rays is subject to temporal variations. These fluctuations are correlated inversely with the solar activity and the strength of the geomagnetic field of the earth (Zreda et al., 2008). Fluctuations of neutron intensity can be of long-term or short-term influence. Using the neutron intensity of neutron monitors which measure the incoming high-energy neutrons, this influence can be corrected. Several neutron monitors are spread over the world and are sensitive to the solar and magnetic variations, but insensitive to local water pools, e.g., soil moisture, lakes etc. (Zreda et al., 2008). The correction factor ( $f_i$ ) normalizes the CRS neutron intensity to the nearest neutron monitor intensity (Zreda et al., 2008):

$$f_i = \frac{I_m}{I_0} \quad (3.7)$$

$I_0$	mean intensity of the incoming neutrons in the calibration period	[cph]
$I_m$	measured neutron monitor intensity	[cph]

**Combination of the Corrections** After the computation of the correction factors, the quality controlled neutron intensity ( $N_{uncorr}$ ) is set off against the correction factors ( $f_p, f_{WV}, f_i$ ). The corrected neutron intensity ( $N$ ) can be used to calculate the subsequent calibration function (Zreda et al., 2012):

$$N = N_{uncorr} * \left( \frac{f_p * f_{WV}}{f_i} \right) \quad (3.8)$$

**Calibration** There are three approaches to calibrate a CRP. The first approach was developed by Desilets et al. (2010) and is simple and applicable in its implementation. They found this calibration approach by modeling the neutron flux with a MCNPX modeling for a site in the COSMOS project, Southeastern Arizona (USA). The equation is “simple, monotonic [and] nearly invariant with soil chemistry [...] and texture” (Zreda et al., 2012):

$$\theta(N) = \frac{a_0}{\left(\frac{N}{N_0}\right) - a_1} - a_2 \quad (3.9)$$

$N_0$  count rate of neutrons at the calibration time under same conditions [cph]

$a_i$  fitted parameters

Equation 3.9 contains three fitted parameters (describing the soil moisture dependence of near-surface neutron intensity), the neutron intensity at the calibration time ( $N_0$ ) and the actual corrected neutron intensity ( $N$ ). For calibration, this equation is usually solved for  $N_0$  with a mean  $\theta$  of soil sampling. Using of this calibration data set, “ $N_0$  becomes a site specific calibration parameter that implicitly includes the effects of lattice water, vegetation, and soil organic carbon inside the cosmic-ray footprint” (Shuttleworth et al., 2013).

Another approach is the universal calibration function, defined by Franz et al. (2013a) for environments in which soil sampling is difficult due to stony environment, inaccessible relief or urban sites (when the approach after Desilets et al. (2010) is unusable due to its necessity of soil sampling). In this approach, the sum of hydrogen moles for different hydrogen signals in the footprint (water vapor, soil lattice water, soil organic carbon, and above-ground biomass) is used:

$$hmf = \frac{H_\tau + H_{SOC} + H_\theta + H_{AGB}}{NO + SiO_2 + H_2O_\tau + H_2O_\theta + C_6H_{10}O_5 + H_2O_{AGB}} \quad (3.10)$$

$$\frac{N}{N_s} = 4.486 * \exp(-48.1 * hmf) + 4.195 * \exp(-6.181 * hmf) \quad (3.11)$$

$hmf$	hydrogen molar fraction	$[\frac{mol}{mol}]$
$H_\tau$	hydrogen moles of lattice water equivalent	$[mol]$
$H_{SOC}$	hydrogen moles of soil organic carbon lattice water equivalent	$[mol]$
$H_\theta$	hydrogen moles of pore water	$[mol]$
$H_{AGB}$	hydrogen moles of vegetation	$[mol]$
$NO$	moles of the air	$[mol]$
$SiO_2$	moles of the soil	$[mol]$
$H_2O_\tau$	moles of lattice water equivalent	$[mol]$
$H_2O_\theta$	moles of soil organic carbon lattice water equivalent	$[mol]$
$C_6H_{10}O_5 + H_2O_{AGB}$	moles of above-ground biomass	$[mol]$
$N_s$	time constant, site specific calibration parameter	$[cph]$

The third calibration approach is the COsmic-ray Soil Moisture Interaction Code (COSMIC), developed by Shuttleworth et al. (2013). This code is based on a MCNPX model, but runs much faster and was developed especially for the calibration of a CRP. It is a physically-based model which includes the degradation of the incoming high energy neutron flux with soil depth, the creation of fast neutrons at each depth in the soil, and the scattering of the resulting fast neutrons before they reach the soil surface (Shuttleworth et al., 2013). The parameterization is done by the chemistry and moisture content of the site specific soil. In Baatz et al. (2014) the three calibration approaches were tested and compared on a humid forest ecosystem in Germany. A validation of the calculated soil moisture derived from CRS with field conditions can be done by a comparison of the integral soil moisture in the footprint to the integral value of the soil moisture of a distributed sensor network, consisting of TDRs or similar devices (Franz et al. (2012a), Franz et al. (2013a) and Bogena et al. (2013)).

### 3.4 Water Management Modeling

To avoid further overexploitation of the aquifers, effectiveness of irrigation or recharge of groundwater should be increased. On the study site cultivated by citrus, main water losses are constituted by the actual evapotranspiration and deep percolation (Amenzou et al., 2013).  $ET_a$  is governed by the transpiration of the trees and their water demand. Deep percolation is governed by irrigation and water loss due to evapotranspiration. Thus the irrigation is a sensitive parameter to influence the  $DP$ . A sustainable irrigation is governed by regulation and understanding the

following questions: how much water can be held by the crop in the root zone? How much water is required daily by the crop? When does irrigation take place? (Newman, 2012). In semi-arid landscapes it is difficult to find the best way between reduction of irrigation water and lift of the groundwater table level. For decision making it is important to regard the water resources used for irrigation. When ubiquitous surface water is used, deep percolation can be increased by irrigation because it does not use groundwater. When the irrigation water is delivered from groundwater pumping, irrigation efficiency should be raised to protect the groundwater table. With an irrigation water management modeling amounts of deep percolation can be calculated and assessed for their efficiency. For modeling different irrigation management approaches, the water balance sheet WatBal V. 3.0 developed by Baroni and Gandolfi (2009), was used (appendix IV).

An indicator for the sufficient water supply to the plants is a minimal or missing difference between  $ET_c$  and  $ET_a$ . If  $ET_a$  falls beneath  $ET_c$  plants suffer water stress. To obtain this information, the evapotranspiration was calculated by the model. The  $ET_0$  was calculated after Penman-Monteith and multiplied with a crop factor  $K_c$  to obtain  $ET_c$ , the potential evapotranspiration for a special crop.

$$ET_0 = \frac{0.408\Delta(R_n - G) + \gamma \frac{900}{T+273} u_2(e_s - e_a)}{\Delta * \gamma(1 + 0.34 * u_2)} \quad (3.12)$$

$ET_0$	reference evapotranspiration	$[\frac{mm}{d}]$
$u_2$	wind speed, at 2 m height	$[\frac{m}{s}]$
$e_s$	saturation water vapor	$[kPa]$
$e_a$	actual water vapor	$[kPa]$
$\Delta$	slope vapor pressure curve	$[\frac{kPa}{^{\circ}C}]$
$\gamma$	psychrometric constant	$[\frac{kPa}{^{\circ}C}]$

$K_c$  responds to the difference in ground cover, canopy properties and aerodynamic resistance of the crop in comparison to a well-watered reference grass.

The actual evapotranspiration was calculated by the multiplication of the  $ET_c$  with the water stress coefficient  $K_s$ . It is a “dimensionless transpiration reduction factor dependent on available soil water” (Allen, 1998).

$$K_s = \frac{TAW - Dr}{TAW - RAW} \quad (3.13)$$

$TAW$	total available water	[mm]
$Dr$	root zone depletion	[mm]
$RAW$	readily available water	[mm]

When soil moisture is at or near field capacity, then  $K_s$  is at or near 1. Thus  $ET_a$  equals  $ET_c$  or is nearly in the same range. With sufficient irrigation those conditions often occur. When  $SM$  is lowered, root zone depletion (water shortage relative to field capacity) falls beneath the readily available water (fraction of TAW that a crop can extract from the root zone without suffering water stress) and  $K_s$  will be reduced until it reaches zero. When soil moisture reaches permanent wilting point  $ET_a$  also yields zero because the plants die and cannot transpire anymore (figure 3.5).

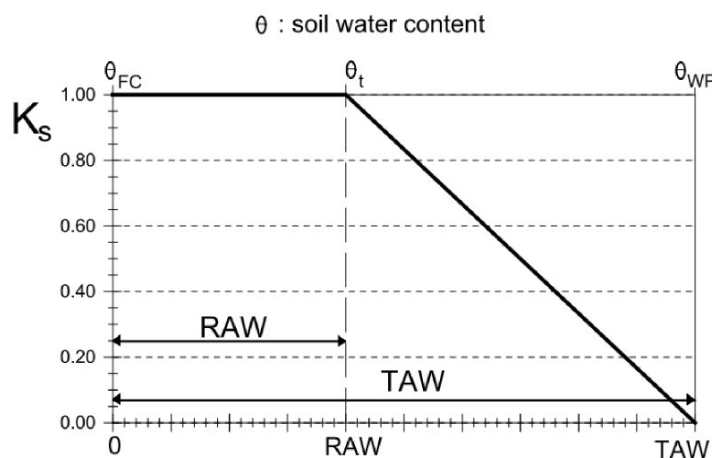


Figure 3.5: Calculation of the water stress coefficient: when soil moisture drops below a certain threshold, root zone depletion exceeds readily available water and  $K_s$  decreases.

For the calculation of water stress conditions and their avoidance crop parameters, soil texture information and irrigation management performance are necessary information for the quantification of the SWB in the model.

Different types of crop are described by parameters as the duration of different crop stage (in days), the leaf area index (for different crop stage), the  $K_c$  (for different crop stage), the minimum and maximum root depth and other three crop parameters<sup>5</sup>.

Soil texture is adjustable for the usual classes and sets parameters like field capacity, wilting point and initial water content in the model.

The model is used to test different irrigation approaches to quantify deep percolation and to meet plant water demands. Therefore it contains four irrigation management approaches: no irrigation, fixed irrigation (certain irrigation amount at fixed date), automatic irrigation (irrigation amount defined by its efficiency, starts when a defined water content threshold is

<sup>5</sup>p=average fraction of Total Available Soil Water (TAW), a= coefficient for the calculation of the amount of rain which contributes to interception, k= factor for the calculation of the cover fraction.

undershot) and irrigation by sprinkler or basin (certain amount of irrigation, starts when a defined water content threshold is undershot). For fixed irrigation eight days of with a certain irrigation amount can be set. The choice of this option requires information and understanding of the meteorological conditions and the resulting plant water requirements to plan the dates of irrigation. The automatic irrigation is governed by the efficiency ( $\eta$ ) and the threshold ( $\alpha$ ). The parameter  $\eta$  is the ratio between the water stored in the soil-root-system to the water applied by the irrigation system. The higher the efficiency the more water is taken up by the roots and not lost by deep percolation. The parameter  $\alpha$  is the fraction of TAW beneath water is not accessible anymore for the plants. When a certain fraction (threshold) is undershot, then irrigation starts to keep the SM in the range of TAW. For the choice between sprinkler or basin some additional parameters had to be set. As mentioned before  $\alpha$  and the kind of delivery have to be set. Additionally the frequency of irrigation (days) and the amount of irrigation applied on the orchard have to be chosen.

The result of the modeling is the number and amount of irrigation and the induced deep percolation under given climatic conditions.



# 4 Experimental Site and Field Activities

## 4.1 Experimental Site

The studied citrus orchard ( $N\ 31^{\circ}29'50.54''\ E\ 8^{\circ}14'37.49''$ ) was established in July 2000 and in 2009 a research station of the University of Marrakesh was installed on it. The orchard was planted with Clementines (Afourer variety). The area covers a size of around 200 ha at a height of 464 m a.s.l.. Citrus trees are of uniform height due to annual pruning. There were planted in rectangular sections with a rows distance of six meters and four meters within the rows (figure 4.1).

The investigated part of the orchard ( $\sim 30$  ha) is situated in an agricultural used area southwest of Marrakesh. Due to an intensive groundwater usage in the last century the groundwater table beneath the area is lowered up to around 43 m beneath surface (figure 2.1).

The orchard is split in three different sectors, which are watered successively in two-hour-intervals, two times a day from 6 a.m. to 6 p.m.<sup>1</sup>. The two-step irrigation is performed to meet peak water requirements of the citrus trees and to avoid high water potentials in the soil<sup>2</sup> or run off. The amount of irrigation depends on the evapotranspiration, measured by a class-A-pan, installed on grass vegetation, at a meteorological station. The amount of irrigation water should exceed the water requirement of the trees for nearly 20 %, because high evapotranspiration leaves salt in the soil, which should be leached to protect the plants from salination phenomena.

The irrigation is performed by surface drippers, located on two sides of the trees with a distance of 1.5 m between the water pipes and 1.0 m between the drip holes in line (figure 4.1). Small paths are located between the lines of trees, which are used for plant management like harvesting, pruning or pest control. Water supply comes from surface water of the reservoir Lalla Takerkoust (located 19 km southeast of the orchard) or from pumping groundwater<sup>3</sup>. The irrigation pattern leads to very heterogeneous soil moisture conditions with dry spots (roads, directly at the trees, middle of the rows) and wet conditions (dripper, parts of the rows).

As a result of fluvial transport of mountainous rock material to the plain, the soil is a stony,

---

<sup>1</sup>Irrigation times: sector 1= 06.00 - 08.00 (a.m.), 12.00 - 02.00 (p.m.); sector 2= 08.00 - 10.00 (a.m.), 02.00 - 04.00 (p.m.); sector 3= 10.00 - 12.00 (a.m.), 04.00 - 06.00 (p.m.)

<sup>2</sup>When soil dries out this leads to a higher soil water potential and water uptake by the plant is limited due to the higher power that is needed, to take up the water. By a two-time irrigation, lower water potentials in the soil make it easier for the trees to take up the water.

<sup>3</sup>Workshop notes from the Kick-off workshop on 19.03.2013 in Marrakesh

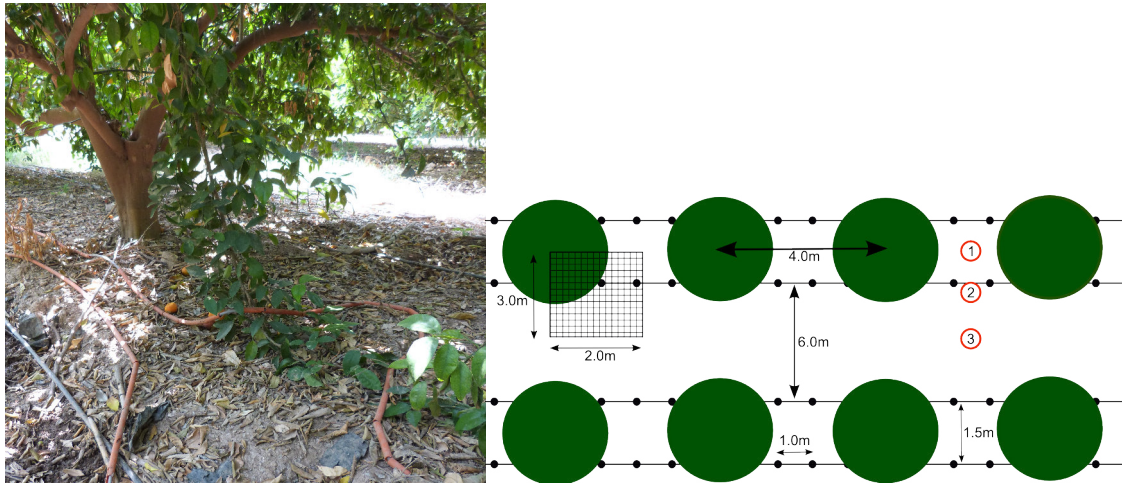


Figure 4.1: Pattern of linearly planted tree lines with irrigation tubing. Additionally the locations of the sampling strategies one (1 = trees, 2=dripper, 3=rows) and two (grid of FDR measurements) are shown.

sandy loam which consists of 20.7 % clay, 35.0 % silt and 44.3 % sand (compare table 5.2). The soil is quite poor in humus, shallow and very skeletal (Müller-Hohenstein and Popp, 1990).

The team of the Cadi Ayyad University in Marrakesh is conducting scientific investigations for the estimation of water transport in the plant-soil-system of the orchard. For this aim, several scientific devices were installed on two locations: a meteorological station installed on grass vegetation where parameters like wind speed and –direction, precipitation, solar radiation, temperature and humidity are being measured. Those parameters are used to calculate reference evapotranspiration according to equation 3.12. The second spot is in sector 2 where a measuring tower was installed with an eddy covariance system. It consists of a 3 D sonic anemometer, a humidity sensor and a hygrometer for measuring the actual evapotranspiration in the field (more descriptions in section 3.2). Nearby, a TDR (installed near a citrus tree with detectors in depths of 5, 10, 15, 20, 40, 60, 80 and 100 cm), a fluxmeter (for measuring the percolation in the root zone of a citrus tree), a heat plate (for measuring soil heat flux) and a net radiometer (for measuring net radiation) are installed. A detailed description of the setup and the devices can be found in Er-Raki et al. (2012).

## 4.2 Soil Water Balance

The measurement of all components of the soil water balance (section 3.1) was conducted on the orchard. An FSS500 tipping bucket automatic rain gauge (Campbell Inc., USA) measures the precipitation at 1 Hz. Daily irrigation is calculated from the amount of water, measured by the water meter on the pumping station. Surface runoff will be neglected due to the flat relief on the orchard. The soil water content is measured by CRS, which is described in more detail in section 4.4. Additional soil moisture measurements on point scale are done by a TDR close to

the measurement tower. The  $ET_a$  is measured by the eddy covariance technique whose setup is explained in detail in the following section.

### 4.3 Eddy Covariance Technique

The ECT system is installed on a tower in the middle of sector 2 (red point in figure 4.4). It consists of a 3D sonic anemometer (CSAT3, Campbell Scientific Inc.) and an open-path ultraviolet krypton hygrometer (KH20, Campbell Scientific Inc.), installed in a height of 8.50 m (figure 4.4). The  $ET_a$  is deduced from the measured latent heat flux  $\frac{W}{m^2}$ , which is calculated with the software package ECpack (done by partners at University of Marrakesh). Therefore latent heat is first converted from  $\frac{W}{m^2}$  to  $\frac{MJ}{m^2 \cdot d}$  by multiplication with the conversion factor 0.0864 and then converted into  $\frac{mm}{d}$  by multiplication with the conversion factor of 0.408 (Abtew and Melesse, 2013). The performance of flux measurements by ECT can be assessed by the energy balance closure (figure 4.2):

$$LE + H = Rn - G \quad (4.1)$$

$LE$	latent heat	$\left[\frac{W}{m^2}\right]$
$H$	sensible heat	$\left[\frac{W}{m^2}\right]$
$Rn$	net radiation	$\left[\frac{W}{m^2}\right]$
$G$	soil heat flux	$\left[\frac{W}{m^2}\right]$

For the present study the coefficient of determination of 0.9118 gives a high accuracy of the ECT measurements. The closure evaluates whether the sum of the estimated latent heat and sensible heat are equivalent to all other energy sinks and sources and thus the uncertainty of the measurement.

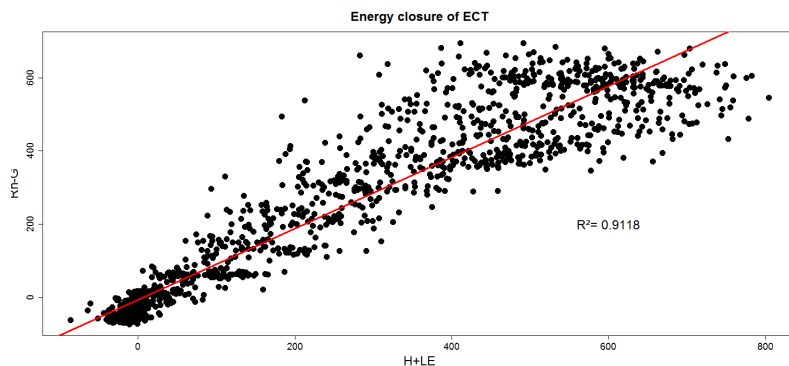


Figure 4.2: Energy closure of the eddy covariance measurements.  $Rn$  is net radiation,  $G$  is soil heat flux,  $H$  is sensible heat flux and  $LE$  is latent heat flux.

## 4.4 Cosmic Ray Probe

The CRP was installed on the same tower as the ECT on 13th of June 2013 on the citrus orchard. It was mounted in a height of six meters, 1.20 m above the canopy (figure 4.4).

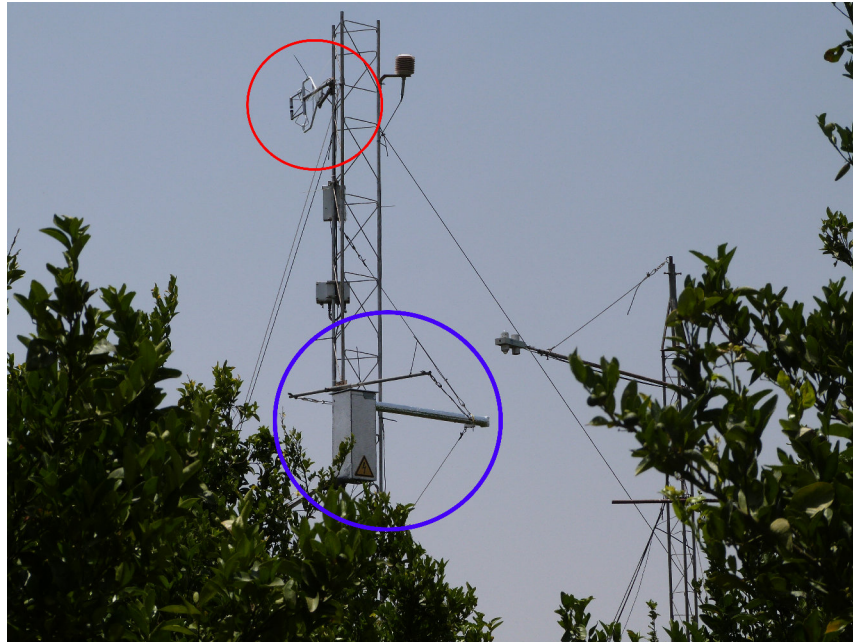


Figure 4.3: Tower in sector 2 with the eddy covariance measurement device (red circle) and the cosmic ray probe (blue circle).

The probe consists of an aluminum box where a polyethylene moderated,  $\text{He}^3-$  gas filled aluminum counter (CANBERRA Industries) is installed horizontally. Inside the box are a detector for the counting of the neutron intensity and its storage. The counting interval was set to 30 minutes. Additionally, a HOBO<sup>®</sup> data logger (Onset Computer Corporation) was installed to measure parameters like temperature, air pressure and air humidity which are needed for the corrections. A small car battery was mounted and connected to a solar panel to ensure the power supply in case of a blackout of the solar panel.

The footprint covers an area of around 30 ha (visible in figure 4.4) on the orchard which is situated in different irrigation sectors: sector 1 (covers  $\sim 7.5$  ha), sector 2 ( $\sim 11.5$  ha), sector 3 ( $\sim 2.0$  ha) and remaining irrigated areas ( $\sim 4.0$  ha). Furthermore, it covers around 3 ha of agricultural roads which are not being irrigated and thus have very low soil moisture contents.

### 4.4.1 Correction of the Neutron Intensity

For the correction of the neutron intensity (after the procedure, mentioned in section 3.3.3) and the following computations, the 30-minutes neutron counts were accumulated to an integration time of one hour. The same time interval was chosen for the meteorological parameters from the HOBO<sup>®</sup>logger.

The corrections were conducted for neutron counts of the calibration time and recent time series.

For atmospheric pressure correction, the attenuation coefficient  $L$  with a range recommended by Zreda et al. (2012) was tested on sensitivity at the local site. The mean value of neutron counts did not change with varying  $L$ . Solely the minimal and maximal values varied less than one percent. Thus the mean value of the range ( $128 \frac{g}{cm^2}$  at high latitudes and  $142 \frac{g}{cm^2}$  at low latitudes) was chosen ( $135 \frac{g}{cm^2}$ ) to avoid a time consuming calculation.

For the correction of the incoming neutrons, the galactic neutron intensity from the neutron monitor in Castilla la Mancha, Spain (708 m a.s.l.) which is the closest to the study site, was used and hourly data were downloaded from the Neutron Monitor Database (Neutron Monitor Database, 2013). The correction was done by using the mean counts per hour from the neutron monitor of calibration time ( $I_0$ ) and the recent neutron counts per hour ( $I$ ).

For water vapor correction, the absolute humidity was calculated after Rosolem et al. (2013) from temperature, atmospheric pressure and relative humidity. Due to a data logger breakdown from 9th of October until de-installation of the CRP, atmospheric pressure data from the airport Marrakesh, Menara (Deutscher Wetterdienst, 2013) and temperature and relative humidity data from the eddy covarianz tower were used. They were normalized to measuring inaccuracies between the HOBO® logger and the external logger.

#### 4.4.2 Calibration of the CRP

As mentioned above, there are three approaches to calibrate a CRP. In the present study, the approach of Desilets et al. (2010) (equation 3.9) was chosen due to its simplicity and applicability. The equation has two variables and three parameters:  $N_{corr}$  are neutron counts per hour, which are corrected for the atmospheric pressure, incoming neutrons and water vapor, while  $N_0$  are (also corrected) neutron counts per hour at the time of calibration. The fitted parameters express the dependence of soil moisture to the near-surface fast neutron intensity, where  $a_0 = 0.0808$ ,  $a_1 = 0.372$  and  $a_2 = 0.115$  (Desilets et al., 2010). This approach is valid if  $\theta \geq 0.02 \frac{kg}{kg}$  and soils are derived from silicate rocks (Desilets et al., 2010).

As recommended by Franz et al. (2013a), the **first sampling** procedure follows a given pattern: 18 sampling positions are located at three different radial distances (25, 75, 200 m), in six different directions (with angels of  $60^\circ$ ) from the probe (figure 4.4). Due to the variation of soil moisture within the depth profile, the sampling proceeds in five centimeter steps, from the surface to 40 cm depth (Franz et al., 2013a). As a result of this sampling pattern, 126 soil samples can be generated in a sampling campaign. Due to unfavorable conditions in the actual study, only 105 samples (plots E1 and E3 not sampled) were taken. One important constraint for the sampling campaign is a duration of maximum six hours: a longer sampling can lead to a larger variation of soil moisture. Especially under the given (semi-)arid climatic conditions, the  $SM$  can have a large variation during the day (Zreda et al., 2012). The time of soil sampling (and thus of

calibration) was the 14th June 2013 from 9 a.m. to 5 p.m..

The above mentioned sampling pattern can be used for homogeneous conditions, where similar values for soil moisture can be expected at all sampling points, contributing equally to the mean soil moisture of the field. However, under inhomogeneous conditions like on the studied orchard with alternating extremely dry and moist areas, a fitted calibration approach has to be used. As recommended by Franz et al. (2013b), an altered design was developed, resulting in specific sampling locations. Those are divided in three different types of moisture contents: at the *dripper*, near the *trees* (between the dripper lines) and in the *rows* (between the irrigated tree lines) (figure 4.1). These sampling locations were distributed consistently on all positions of the traditional sampling design.

The soil cores were taken with a split tube sampler (Eijkelkamp Agrisearch Equipment) which produces undisturbed soil cores with an inner diameter of 4.8 cm. Since the split tube contains a reusable sample liner of PVC that wraps the soil, the soil cores stay undisturbed while sampling. Soil cores were cut in five centimeter pieces, weighed and packed in plastic bags to avoid evaporation.

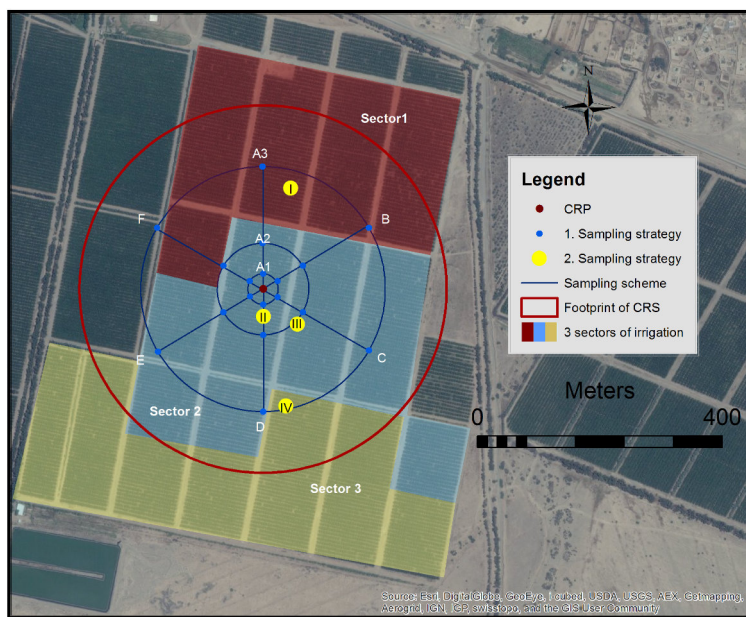


Figure 4.4: Size of the CRS footprint and sampling pattern of campaign one. The blue points are the drilling positions of the first sampling campaign (designed after Franz et al. (2013a)) and the yellow points the ones of the second campaign.

For the calculation of the soil moisture the soil samples were weighed, dried for 24 h at 105°C, weighed again and sieved (with a mesh size of 2 mm to extract the gravel).

All soil analyses were conducted in the laboratories of the Faculté des Sciences Semlalia, Marrakech.

With the radius ( $r=2.4$  cm) of the driller and height of the soil core ( $h= 5$  cm) the volume of the sample ( $V_c$ ) is calculated by:

$$V_C = \pi * r^2 * h \quad (4.2)$$

$r$  radius of the driller [cm]  
 $h$  height of the single soil core [cm]

Bulk density ( $\rho_{BD}$ ) can be calculated by the volume and weight of a sample. By multiplication of the gravimetric water content with bulk density, the soil moisture ( $\theta$ ) can be calculated:

$$\rho_{BD} = \frac{m_t}{V_C} \quad (4.3)$$

$m_t$  weight of 105°C oven-dried soil [g]

$$\theta = \left( \frac{(m_f - m_t)}{m_t} \right) * \left( \frac{\rho_{BD}}{\rho_W} \right) \quad (4.4)$$

$m_f$  weight of wet soil [g]

$\rho_W$  density of water [ $\frac{g}{cm^3}$ ]

For the present method of calibration it is important to include water contents, stored in the crystal lattice or in soil organic matter (SOM), and soil organic carbon (SOC), respectively, since these additional water pools influence the moderation of neutrons. Their influence on the neutron intensity is highest for very dry soils, where the soil moisture is low (Franz et al., 2013a).

Lattice water is stored in the crystal lattice of clay and silicate minerals in the soil and is relatively constant over large time scales like thousands of years. Water stored in the SOM is located in living or dead organic material like plants, roots or animals etc. and is mostly influenced by the climate, soil texture, land use and vegetation. It also changes only slightly over large time spans. From the SOM, the SOC can be calculated by the division of the conversion factor 1.72 (Blume et al., 2011).

To assess the amount of water stored in the organic carbon, the loss on ignition was calculated by weighing the 105°C dried samples, glowed for 24 h at 550°C and weighing them again. Only a selected number of samples were dried, due to the energy- and time-consuming procedure. A mixed sample of different depths from different locations was dried in duplicate. The loss on ignition was calculated by the mean of the two samples of each location and the mean of those three locations (*dripper*, *trees*, *rows*) was taken for the calculation of SOC (Franz et al., 2013a):

$$SOC = \frac{\left( \frac{m_t - m_{550}}{m_t} * 100 \right)}{1.724} \quad (4.5)$$

$m_{550}$  weight of 550°C oven-dried soil [g]

For determination of lattice water the same procedure as for organic carbon analysis was applied. However, for this analysis the soil was dried for 24 h at 1000°C (Zreda et al., 2012).

To obtain additional information of the extent of the areas with different wetness conditions, a **second soil sampling** campaign was conducted on 8th of December 2013. To quantify the distribution of the soil wetness, the smallest unit of the orchard was taken as an example-plot: a grid with an extent of two to three meters (from a citrus tree to the middle of the ways and the irrigated rows). The single parcels of the grid had an extend of 10 cm in height and lenght (grid in figure 4.1). In those grids, sampling was done with an FDR WET-2 Sensor (Delta-T Devices). One drilling and FDR sampling in each irrigation sector (plot I, II, IV in figure 4.4) and one additional FDR sampling in sector 2 (plot III in figure 4.4) were conducted. The drilling was done with the above mentioned split tube driller on the three mentioned locations (*dripper, trees, rows*). At plot III, the FDR measurement was done on the surface and on a ten centimeter deep trench to analyze the moisture structure below the surface. During sampling, irrigation occurred or started after some time of measuring on each plot and thus there was influence of irrigation on every plot.

Due to the linearly arranged planting and irrigation of the citrus trees, there is a strong heterogeneity in soil conditions and moisture contents on the orchard. To account for these characteristics, horizontal and vertical weightings of the soil moisture were done. First, the horizontal diversity was quantified for the single locations (*dripper, trees, rows*). The soil moisture of the 16 locations from the first sampling campaign (layer by layer) was multiplied with the areal proportion of the three locations to the total area of the orchard. The proportions were quantified by FDR measurements during the second campaign.

The depth layers ( $z$ ) used for soil moisture calculation were the layers between surface and penetration depth ( $0 < z < z^*$ ). A linear depth weighting function, developed by Franz et al. (2012b), was used to account for the bigger influence of neutrons from upper layers (equation 3.4). For this aim, a depth weighting factor  $wt(z)$  was calculated for every centimeter of depth and then summed up for five centimeter-steps (to obtain same depth setups as by drilling). The weighting factor was multiplied with the soil moisture of the according layer. These depth-weighted soil moistures are vertically summed up and yield the final soil moisture for the calibration time.

For a better knowledge of soil characteristics, the **soil texture** was determined by laser scattering particle size analysis. With the use of a LA-300 Laser Diffraction Particle Size Distribution Analyzer (HORIBA Instruments Inc.), 22 samples from different locations in the footprint were examined.



## 5 Results

### 5.1 Cosmic Ray Neutron Counts and Calibration

During the period of measurements, neutron intensity, detected by the CRP, had a range of 536.6 counts per hour *cph* to 939.7 *cph* and showed short- and long-term variability (figure 5.1). Compared to studies of Zreda et al. (2012), Rosolem et al. (2013) or Franz et al. (2013a), local neutron counts obtained from the experimental site are low and show smaller variability. There are three gaps of neutron counts in the time series: early July (three days), end of July to August (14 days) and middle of September (five days). Two of these gaps coincide with the biggest rain events in the time series. Consequently there are no information about the changes in neutron intensity during such intensive rain events. The gap of long duration is induced by a cable problem while reading out data. The other two gaps (which coincide with the heavy rain events) may be caused by a technical problem with the power supply.

Corrections of raw neutron intensity lead to a slight shift and smoothing of the signal with increasing influence from the middle of October (figure 5.1). Peaks and outliers are smoothed by the correction factors and neutron intensity shows a smaller variability.

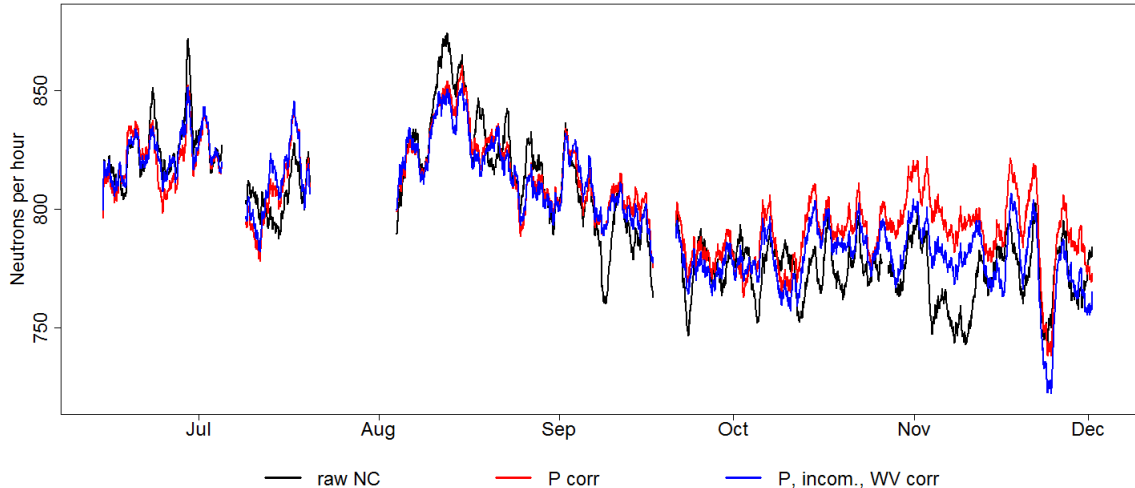


Figure 5.1: Raw and corrected neutron counts per hour, smoothed by a 24-hour moving average. Shown is the raw intensity (raw NC), pressure corrected (P corr) and for all influences corrected neutron intensity (P, incom., WV corr).

The high impact of the correction factors, as from the middle of October can be explained by

the usage of meteorological data from another logger. The data from the surrogate loggers were used from 9th of October, due to the breakdown of the installed HOBO® logger.

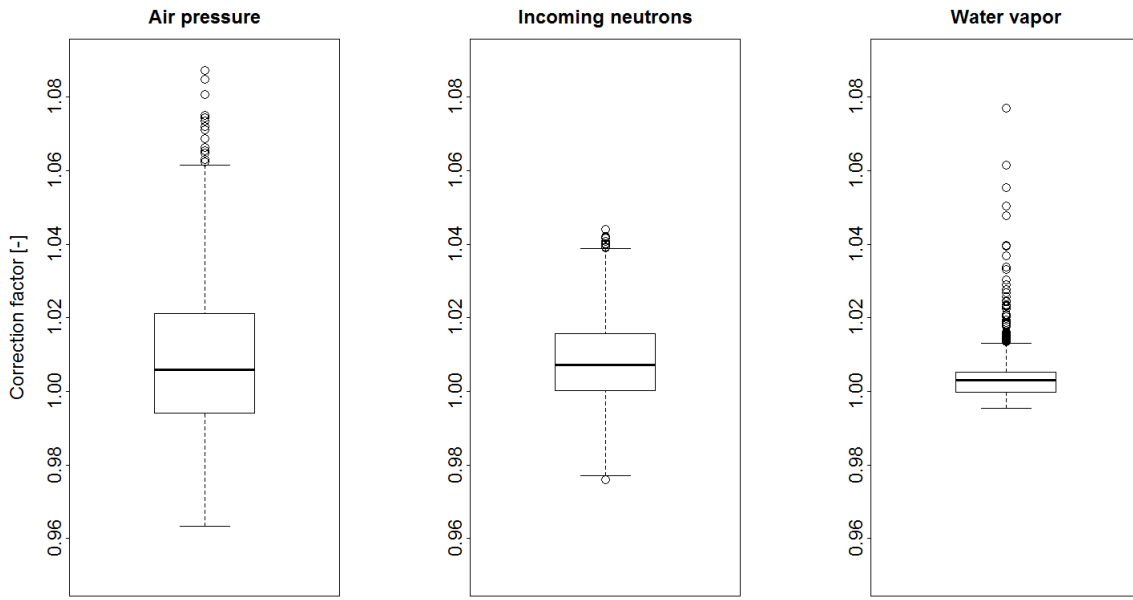


Figure 5.2: Box-plots of the correction factors, calculated after equations 3.5,3.6 and 3.7.

In figure 5.2 a slight fluctuation of the factors around one is visible which is an indicator for the weak influence of the three corrections in all seasons. Especially the atmospheric pressure correction cuts the peaks and flattens the signal, which is also represented by the long whiskers. It has the highest variability (mean: 1.010, standard deviation: 0.021) and thus the highest influence on the neutron correction. The corrections for incoming neutrons (mean: 1.006, standard deviation: 0.011) and water vapor (mean: 1.002, standard deviation: 0.004) have smaller variability and thus lower influence. An influence of galactic neutron intensity on the decreasing CRS signal can be excluded as visible in appendix I. Incoming neutron intensity increases while CRS neutron intensity decreases.

The mean penetration depth of CRS during investigation time was around 15.5 cm with a highly variable range from 8 to 21 cm. With increasing soil moisture from June to December the penetration decreased with the same dynamics.

### 5.1.1 Calibration

The calibration of the CRP was carried out after the approach of Desilets et al. (2010) which needs reference soil samples from the study site. Two soil sampling campaigns were carried out in the above mentioned designs for calibration and quantification of moist areas (chapter 4.4.2). During the first campaign, 16 instead of the recommended 18 plots were sampled and analyzed for the soil moisture, the water content in the mineral lattice and in the soil organic carbon and the soil texture. The mean total water content was  $0.198 \frac{cm^3}{cm^3}$  with a quite high standard

deviation of  $0.099 \frac{cm^3}{cm^3}$ . This high variability is caused by the heterogeneous conditions on the orchard. This VWC was calculated by multiplication of the gravimetric water content with the bulk density of each sample (average for the orchard:  $1.49 \frac{g}{cm^3}$ ). The amount of water, stored in the lattice of the soil minerals, was in spatial average  $0.085 \frac{g}{g}$ . The amount of water, stored in the SOC, was in average  $0.037 \frac{g}{g}$ . The rule that the amount of water equivalent stored in the SOC is about half of the amount stored in lattice water is thus fulfilled (Zreda et al., 2012). The mean soil moisture of the 16 sampling points from 0 to 40 cm was  $0.198 \frac{cm^3}{cm^3}$ . It was used to calculate the penetration depth of the calibration time after equation 3.3 and led to a value of 0.139 m. This value implies that during the calibration time, 86 % of the back scattered neutron intensity was generated on average in a depth of 0 to  $\sim 14$  cm.

Based on the heterogeneous soil moisture conditions on the orchard, horizontal and vertical weighting of the calibration data set was necessary. The horizontal weighting considered the heterogeneous moisture conditions of irrigated and non-irrigated areas. Vertical weighting considered the higher influence of upper soil layers for backscattering and moderating neutrons.

For **horizontal** weighting, information from the second campaign were used for the quantification of the areas with different moisture contents. As mentioned above, areas around the dripper are very moist and areas in the rows and between the trees are much drier. The surficial FDR measurements provided a spatial pattern of *SM* for a typical area of the orchard<sup>1</sup> (figure 5.3).

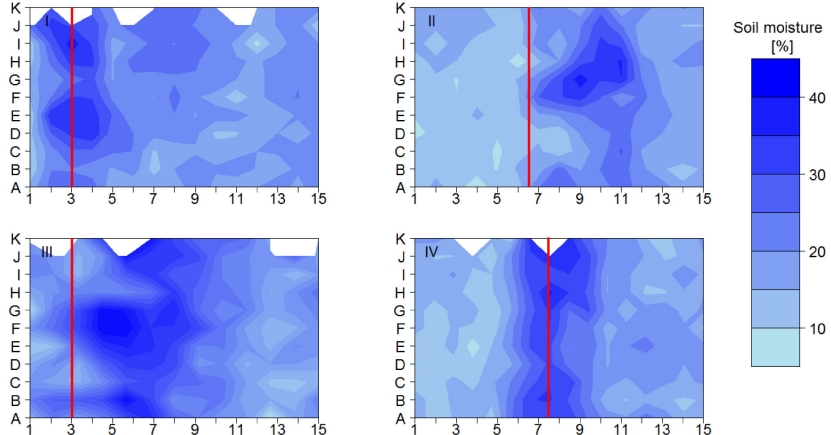


Figure 5.3: Surficial soil moisture for plots I - IV measured with the FDR. Red lines show the irrigation ropes. In each figure the citrus tree is situated in the bottom left corner (A1).

Plots I and IV show similar behavior in the distribution of the *SM*: wetter areas are located close to the drip lines, which are located in different distances from the trees. On plots II and III, higher *SM* values are not restricted to the irrigation ropes and are spatially distributed. These

---

<sup>1</sup>Grid of two to three meters, starting from the tree to the middle of the row. Serves as the smallest representative unit of the orchard.

differences might be induced by surface runoff and ponding water or drying out of the soil by intensive insolation.

To quantify the weighting factors for the three locations (*dripper*, *tree*, *rows*), the spatial distribution of *SM* in plots I and IV was used. Those plots represent the most common conditions in the field which was verified by visual inspection of field conditions. The mean size of wet areas (defined by *SM* contents of 0.25 - 0.45  $\frac{\text{cm}^3}{\text{cm}^3}$ ) around the irrigation ropes was quantified and the remaining areas of *trees* and *rows* calculated.

This definition lead to the following spatial distribution: *dripper* represents 13 %, *trees* 23 % and *rows* 53 % proportion of the area of the CRS footprint. As visible in map 4.4, the orchard furthermore consists of broad agricultural roads with quite dry soil conditions. They represent around 10 % of the area on the orchard.

The **vertical** weighting was conducted with the horizontally weighted *SM* after equation 3.4. The mean weighted soil moisture resulted in a lower value: without weighting the average *SM* for the layers 0 to 15<sup>2</sup> cm was 0.211  $\frac{\text{cm}^3}{\text{cm}^3}$ , weighted (but without the quantification of the agricultural roads) it results to a value of 0.188  $\frac{\text{cm}^3}{\text{cm}^3}$  and after a weighting including the very dry agricultural roads (assuming a *SM* of 0.1  $\frac{\text{cm}^3}{\text{cm}^3}$  for the roads) the value for the mean areal soil moisture for the calibration time was 0.157  $\frac{\text{cm}^3}{\text{cm}^3}$ . By including drier parts of the orchard average integral *SM* decreases for around 0.06  $\frac{\text{cm}^3}{\text{cm}^3}$  and gives a more realistic impression of the predominantly dry conditions (table 5.1).

Table 5.1: Statistical summary of weighted and unweighted soil moisture of calibration data set (in  $\left[\frac{\text{cm}^3}{\text{cm}^3}\right]$ ).

	unweighted <i>SM</i>	weighted <i>SM</i>
Mean	0.233	0.173
Standard deviation	0.042	0.031
Minimum	0.134	0.098
Maximum	0.520	0.369

The unweighted soil moisture is generally higher with a bigger range. Anyway, for the moist autumn those results are obviously too high for an orchard in a semi-arid region. The range of the unweighted *SM* is much higher and leads to a higher variability. It can be assumed that the smaller range of the weighted *SM* represents the conditions in the field better, due to the consistent irrigation and stable weather conditions in the observed time span.

The designation of the three typical locations (section 4.4.2) is confirmed by the depth profiles in figure 5.4: mean values of the locations show characteristically differing behaviors. Even though the profiles of the single locations show high variations. *SM* at the *dripper* shows a slight

---

<sup>2</sup>These depths were used because they represent the mean penetration depth ( $\sim 14$  cm) calculated with the calibration data set.

decrease with depth, at the *trees* a slight increase, and at the *rows* stable conditions with depth. Sample points near the *dripper* have high *SM* in the upper layer which decreases with depth due to regular irrigation on the surface. Different timing of irrigation in the sectors during soil sampling lead to the big range of soil moisture.

Quite stable conditions beneath the *trees* lead to depth profiles with a small range of *SM*. Due to the shading by the canopy and thus low climatic influences (small amounts of precipitation and even just weak variation of insolation while stable irrigated conditions), the range of the *SM* among the different plots is much smaller than the *SM* of the sample points near the *dripper*.

A high range and more or less consistent course of the *SM* depth profiles at the *rows* can be a result of very diverse conditions on the orchard. Partly the surfaces of the *rows* are dried out (bare soil on the surface), partly water drains off and ponds every day to the middle of the row (for example due to a broken drip whole) and grass is growing in those spots. These opposing conditions can lead to this large variability.

On average, the location *dripper* has the highest values of VWC ( $0.251 \frac{cm^3}{cm^3}$ ). *Trees* are the driest sites ( $0.132 \frac{cm^3}{cm^3}$ ) and *rows* have an intermediate value ( $0.217 \frac{cm^3}{cm^3}$ ) because of their highly variable conditions. Already Koo (1961) confirmed common ratios for a citrus orchard in Florida: *trees* were much drier than *dripper* or *rows*.

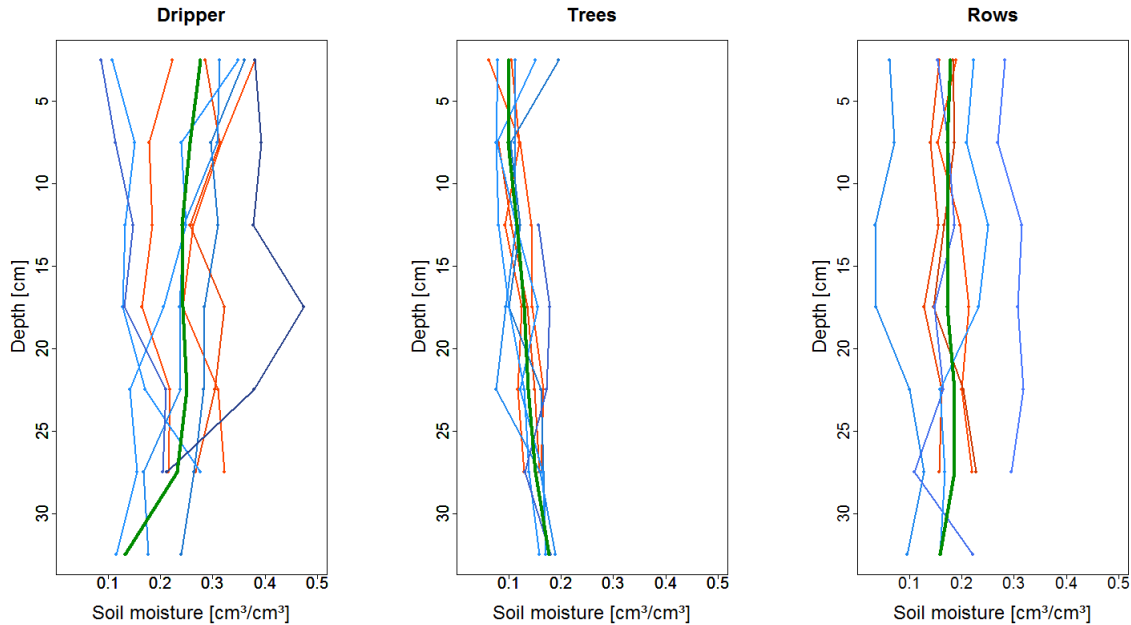


Figure 5.4: Soil moisture values of sampling campaigns one and two, plotted for the depth at the three locations. Depth profiles in blue tones are from the first sampling campaign and red ones from the second campaign. The green lines show the mean soil moisture values.

### 5.1.2 Texture Analysis

The texture was analyzed to obtain additional information of the soil to assess the bottom flux and its distribution processes. For the analysis, 22 samples were taken from different plots of the first sampling campaign. The results were classified after the FAO World Reference Base (Table 5.2). The distribution of the texture in the footprint is predominantly homogenous: most samples consist of a loamy material, except for three samples which consist of sandy or clay loam on the surface. This can be a result of the agricultural treatment of the orchard.

The proportion of stones (soil grains with a diameter  $> 2 \text{ mm}$ ) is on average around 30 % in the sampled soil. The average grain size distribution of the soil is 44 % sand, 35 % silt and 20 % clay. Er-Raki et al. (2012) observed a similar soil composition of the orchard: they described a sandy, loamy texture with 50 % sand, 32 % silt, and 18 % clay. These values result in a field capacity of  $0.26 \frac{\text{cm}^3}{\text{cm}^3}$  and a permanent wilting point of  $0.12 \frac{\text{cm}^3}{\text{cm}^3}$  for a loamy soil (Bundesanstalt für Geowissenschaften und Rohstoffe, 2006).

Table 5.2: Results of the texture analysis with grain size distribution and classification of the soil after FAO World Soil Classification. The position C2 was analyzed for all depths. L= loam, CL= clay loam, SL= sandy loam.

Position	Depth [cm]	Location	Clay [%]	Silt [%]	Sand [%]	FAO
A1	0 - 5	dripper	13.9	35.8	50.3	L
A2	10 - 15	trees	24.3	39.3	36.4	L
A3	30 - 35	rows	23.1	39.9	37.1	L
B1	10 - 15	rows	18.5	32.1	49.4	L
B2	30 - 35	dripper	20.5	31	48.5	L
B3	0 - 5	trees	17.5	38	44.5	L
C1	30 - 35	trees	19.9	35.2	44.9	L
C2	0 - 5	rows	17.9	35.7	46.4	L
	5 - 10	rows	26.1	29.6	44.2	L
	10 - 15	rows	21.2	37.6	41.2	L
	15 - 20	rows	28.8	34.6	36.6	CL
	20 - 25	rows	20.8	32.9	46.3	L
	25 - 30	rows	22	31.8	46.2	L
	30 - 35	rows	20.3	29.9	49.9	L
C3	0 - 5	dripper	12.5	27.7	59.8	SL
D1	0 - 5	trees	28.6	38.4	33	CL
D2	10 - 15	trees	21	41.3	37.7	L
D3	20 - 25	dripper	20.4	41.4	38.2	L
E2	20 - 25	dripper	18.1	33	48.9	L
F1	30 - 35	trees	19.5	37.3	43.2	L
F2	10 - 15	rows	26.2	35.8	38	L
F3	0 - 5	dripper	14.4	32	53.6	SL

## 5.2 Soil Water Balance

The single components of the soil water balance were detected on different temporal and spatial scales. Precipitation, evapotranspiration and soil moisture were measured in half hourly time steps, the irrigation was given in daily time steps. Therefore all components have been aggregated to daily values to have a direct comparison on the same timescale between the inflows and outflows. Precipitation was measured on point-scale whereas the remaining three components were measured on field-scale.

### 5.2.1 Precipitation and Irrigation

The amount and occurrence of precipitation is quite irregular and small which is typical for the climate zone of the study area: a total amount of only 62 mm occurred in the investigation time. During the summer months, only few but heavy rain events occur. The intense rain event on the 8th of July (28 mm) was the only occurrence of precipitation in the first two and a half months of measurement time. In autumn, smaller and more frequent events occurred, even though rainfall remained scarce (figure 5.5).

Since the deficit by actual evapotranspiration highly exceeds the input of water by precipitation, irrigation has to be performed. The amount of irrigation water is assessed by the reference evaporation of a class-A-pan on the orchard. The total amount of irrigation water, applied in the investigation time was 985 mm. On average, the irrigation height was  $5.5 \frac{mm}{d}$ , with only three days without any irrigation (figure 5.5). Predominantly the amount of irrigation was stable for weeks: from June to middle of July around  $6 \frac{mm}{d}$ , in August an average of  $7 \frac{mm}{d}$ , September to middle November  $5.5 \frac{mm}{d}$  and from middle of November onward  $4 \frac{mm}{d}$ . The irrigation amount was in general 20 % higher rated than plant water demand, to leach the mentioned salination of the soil.

### 5.2.2 Evapotranspiration

The actual evapotranspiration measured by the ECT shows a high variability in the observed time: the average  $ET_a$  is around  $4.7 \frac{mm}{d}$  with a standard deviation of  $1.2 \frac{mm}{d}$ . The total amount is 602 mm from middle of June to end of October (14th of June to 21th of October) and it shows a decreasing course (figure 5.5). This course is induced by a smaller soil evaporation and plant transpiration after summer due to lower temperatures, lower insolation and a smaller saturation deficit in the air (appendix II). Due to still remaining data for  $ET_a$ , measured by eddy covariance, the time series is only up to October. As described by Amenzou et al. (2013), the transpiration dominates the amount of evapotranspiration: 80 - 98 % of  $ET_a$  are produced by the citrus trees and thus this value is sensitive to plant growth and development.

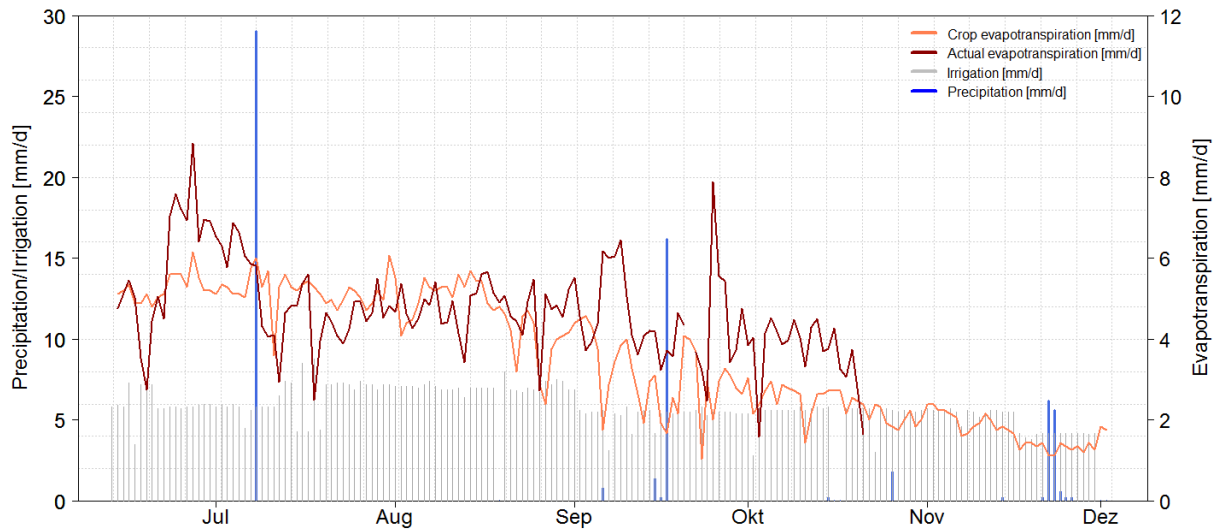


Figure 5.5: Relation between actual and potential evapotranspiration, irrigation and precipitation.  $ET_a$  is measured by the eddy covariance technique and  $ET_c$  is calculated by the WatBal Model. For  $ET_a$ , only data until October were available.

Potential evapotranspiration was calculated for the citrus orchard to gain additional information about the plant-water-relations. A  $K_c$  of 0.6 was found for the present citrus orchard by (Er-Raki, ???).

Measured  $ET_a$  and calculated  $ET_c$  show a similar development. However,  $ET_c$  has a stronger slope in its decrease in autumn which is due to the higher dependency of this variable on the climatically conditions (figure 5.5).  $ET_c$  has to be higher than or equal to  $ET_a$  because the potential evapotranspiration is related to an environment with an unrestricted water supply. If less water is available than is needed by the plants,  $ET_a$  is lower than  $ET_c$  and plant water demands are not covered. This happens in summer months of July and August, when the integral areal water supply is too low for the evapotranspiration demands. From middle of September onwards, the  $ET_a$  and  $ET_c$  are nearly in the same range. Sometimes the actual evapotranspiration exceeds the potential evapotranspiration which is factual not possible. Those difficulties can occur due to the usage of a uniform  $K_c$  during the vegetation periods, due to the different methods of quantification (calculation of  $ET_c/ET_0$  and field measurement of  $ET_a$ ) or due to the effect of soil evaporation during the wetting events. Allen (1998) recommended an adaption of the  $K_c$  to changing vegetative conditions. The usage of a higher  $K_c$  from middle of September onwards would be useful in the actual case because an increased canopy due to growing citrus fruit may also increase the  $K_c$ . Here, an adjustment of  $K_c$  to the different phenological stages was not done because detailed information of phenology are lacking.

When  $ET_a$  exceeds  $ET_c$ , the so-called oasis effect can be the reason. By this effect, sensible heat, originated in the dryer surrounding areas, is transported by 'broadsiding' wind to the orchard and leads to higher evaporation rates. The additional amount of sensible heat is not

included in the calculation of the  $ET_0$  because point measurements were used for its calculation (and did not quantify the high areal influence of sensible heat) and thus it underestimates the evaporative flux.

### 5.2.3 Soil Moisture

Previous to the calculation of the **CRS** soil moisture, calibration was done by solving equation 3.9 for  $N_0$ . Therefore the weighted  $SM$  ( $0.157 \frac{cm^3}{cm^3}$ ) was used and lead to a mean neutron intensity at calibration time ( $N_0$ ) of  $1218 cph$  during calibration time. Afterwards the equation was solved for the actual  $\theta$ . In figure 5.6, weighted and unweighted soil moisture measured by the CRP and TDR  $SM$  are compared. The values were smoothed by a 24-hour-moving average to reduce counting uncertainty. Nevertheless, by smoothing, local extreme values are removed and minima and maxima are not visible anymore.  $SM$  of CRS shows a short and long-term variability on daily, weekly and seasonal scale with a quite high standard deviation (table 5.1).

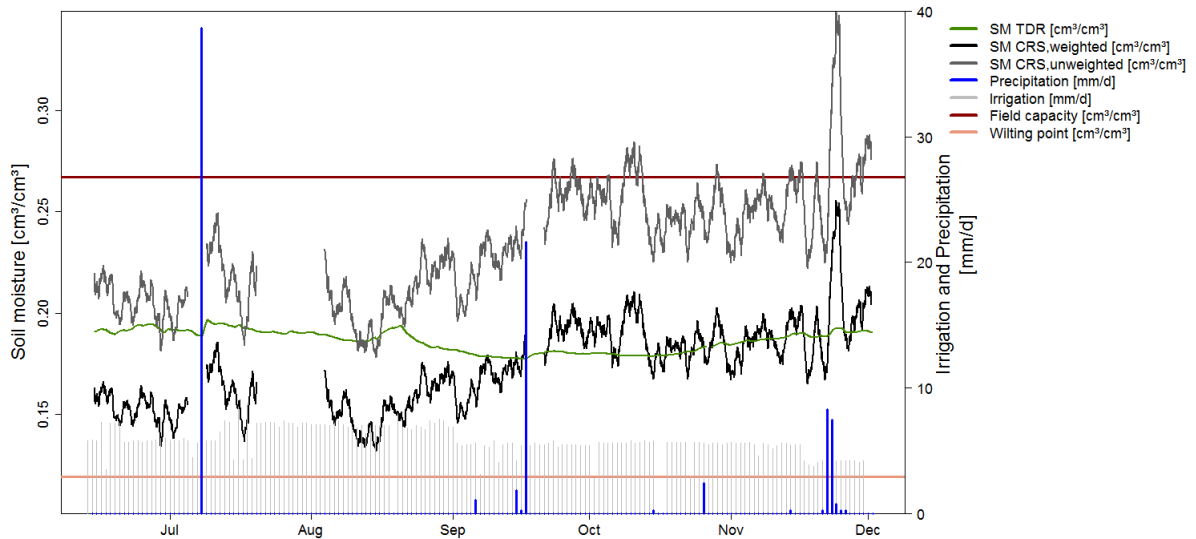


Figure 5.6: Soil moisture measured by TDR and CRS from June to December 2013. For the CRS, unweighted and weighted  $SM$  are shown. Additionally field capacity and wilting point for loam are plotted to show the range of total available water for the citrus trees.

Daily observations showed a high variability and only a weak pattern. In figure 5.7 the residuals of  $SM$  (from June to December) are calculated and shown as boxplots and mean for aggregated hours of the day. In the bottom figure, a slight correlation in comparison with the irrigation times of the orchard is visible (the range of variation is quite small). In the morning, when irrigation starts,  $SM$  increases and reaches relatively stable conditions during irrigation of sector 2. During irrigation in sector 3 mean  $SM$  decreases (while latent heat, which is a direct indicator for  $ET_a$ , increases in this time). This decrease is induced by a drying out of sector 1

and 2 (due to high evapotranspiration) and only a minor influence of the third (irrigated) sector to the footprint. With the second irrigation run,  $SM$  increases again while irrigation in the first sector is conducted, but is decreasing strongly during irrigation of the second and third sector. The steep increase is explainable by the large fraction of sector 1 in the footprint and thus its high influence on the  $SM$  signal. The decrease of  $SM$  while irrigation in sector 2 and 3 can be explained by increasing evapotranspiration in this time which has its mean peak between 12.30 p.m. and 2.30 p.m. A high amount of irrigated water evaporates directly from the soil and  $SM$  declines. Around 7.00 p.m.,  $SM$  starts to increase again because the  $ET_a$  is low (due to missing insolation) so that citrus trees take up less water and less soil moisture evaporates.

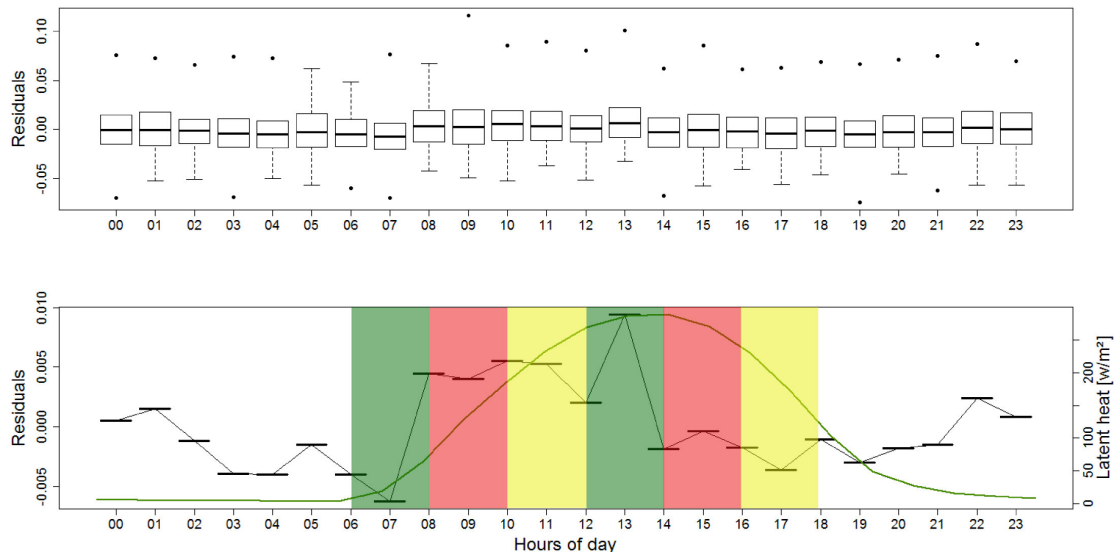


Figure 5.7: CRS soil moisture aggregated for the hours of the day (for the whole investigation time). In the top graph the dispersion for aggregated hours as box-plots; in the bottom graph daily variation of the mean  $SM$  compared with the latent heat (green line, which is a direct indicator for  $ET_a$ ) are shown. Coloured rectangles show the irrigation intervals for the sectors one to three (1=green, 2=red, 3=yellow).

Weekly fluctuations of  $SM$  are quite difficult to explain under given stable hydrological conditions on the orchard. A stable daily irrigation, quite consistent meteorological conditions and only slight rain should lead to a relatively uniform soil moisture (table 5.3). However, in the actual study neutron intensity might be influenced strongly by transpiration rates of the trees which differ significantly in time and under given climatic conditions.

There is also seasonal and interseasonal variability of the  $SM$  observable in the data: from June to beginning of August, high variability around a constant level of  $SM$  occurs (figure 5.6), whereas in August, an increase takes places for more or less one month. From the middle of September, the level of  $SM$  is stable again (with slight fluctuations).

The soil moisture measured by **TDR** between five and 15 cm shows in general a smaller

variability<sup>3</sup>. With a standard deviation of  $0.004 \frac{\text{cm}^3}{\text{cm}^3}$ , the range of the TDR-measured  $SM$  ( $0.177 \frac{\text{cm}^3}{\text{cm}^3}$  to  $0.198 \frac{\text{cm}^3}{\text{cm}^3}$ ) is much smaller than for CRS (figure 5.6 and 5.8). This might be a result

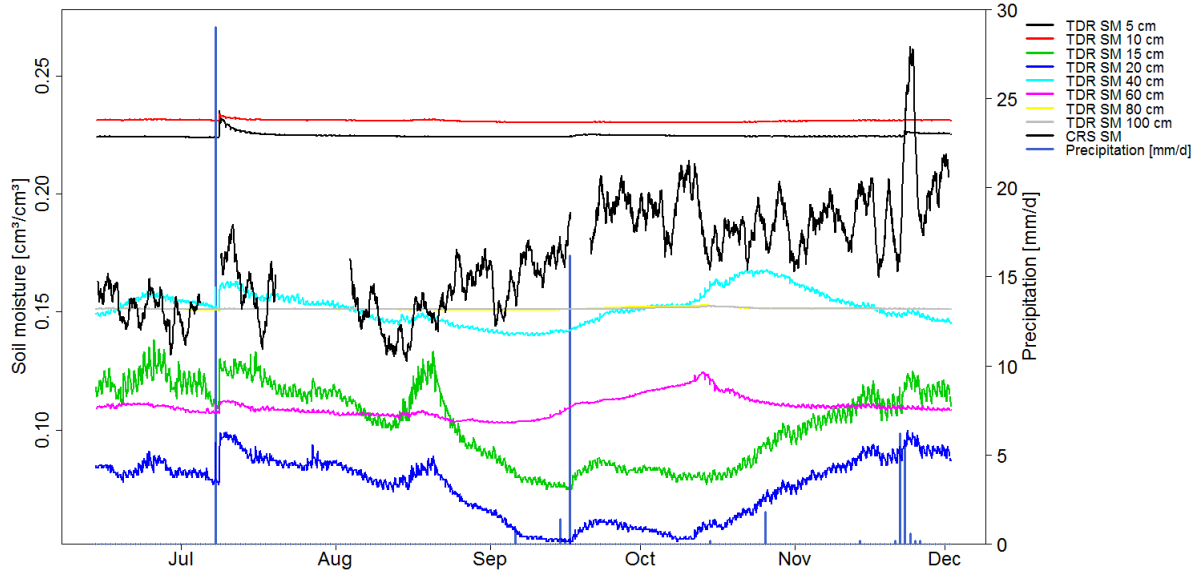


Figure 5.8:  $SM$  in the different measurement depths of the TDR from 0 - 100 cm, compared to the soil moisture of CRS.

of the position of the TDR: only slight influences of precipitation and insolation and in general more stable conditions in the soil occur beneath a citrus tree. Examined separately for the single layers, the behavior of the TDR is not uniform: the upper layers (5 - 10 cm) are consistently moist for the whole period with only a small variability. In contrast, the layers from 15 - 20 cm are driest and have a high variability which is partly induced by heavy rainfalls. From the end of August until the middle of October, a steep decrease of  $SM$  only for these two layers is observable. The high variability of  $SM$  in those layers can be an indication for the highest root density which consumes the majority of water (Newman, 2012). The layers of 40 - 60 cm show a smaller variability and an opposing behavior compared to the two layers above. This can be a result of the more stable conditions of the soil moisture in the zone beneath the root zone. In autumn the values increased because in general more water remains in the soil system. The deepest layers between 80 and 100 cm show a small variability and low moisture contents for the observed time which can be interpreted as a result of only small changes in  $SM$  in these deep layers.

On a daily scale, the TDR shows a quite regular behavior and only a small statistical dispersion (top figure) because of the stable conditions on the location *trees* (figure 5.9). The peak of soil moisture occurs later in the day than that of CRS  $SM$  because its position upside of the dripper

<sup>3</sup>Evaluated by the mean value of layers 5 - 15 cm to have a better comparison with the mean penetration depth of CRS.

towards the tree. Irrigation water needs some time to be transported to the tree by root suction. The TDR *SM* is not highly governed by evapotranspiration because the TDR position is shaded by a citrus tree. In comparison to CRS the *SM* of TDR shows smaller reaction after rain events because the interception water is not measured by TDR. In contrast to the TDR, the CRS measures an additional water pool (interception) and thus shows a steeper increase after rain and due to high evapotranspiration from the leaves also a steep decrease of the *SM* signal (figure 5.6).

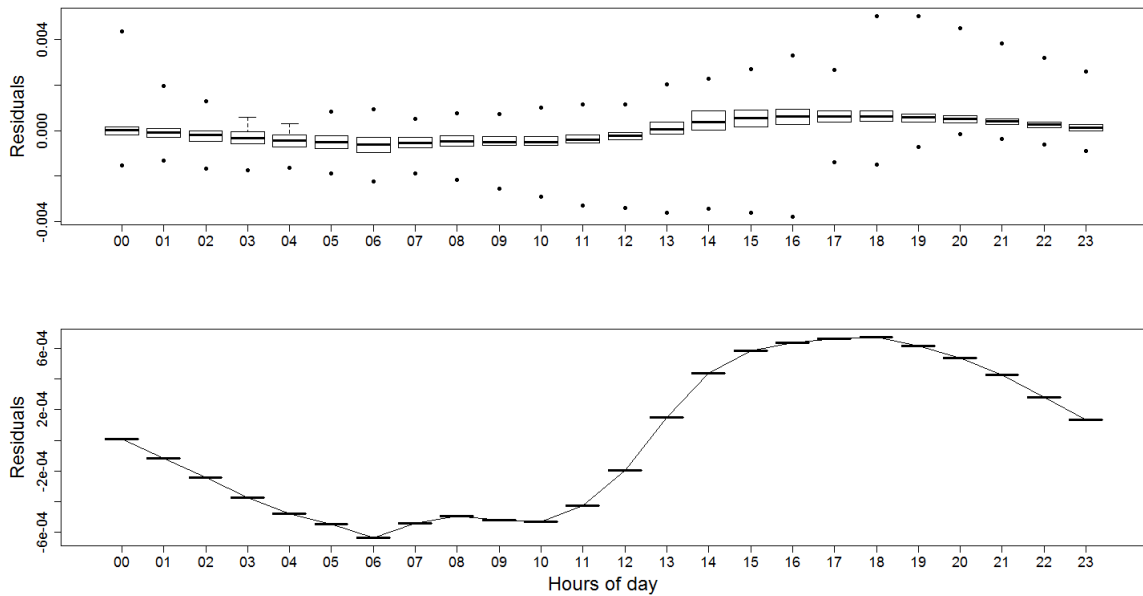


Figure 5.9: TDR soil moisture (for depths 5 - 15 cm) aggregated for hours of the day (for the whole investigation time). In the top graph the dispersion for the aggregated hours as box-plots, in the bottom graph the daily variation of the mean *SM* are shown. Irrigation intervals are the same as the coloured ones in figure 5.7.

On the weekly scale the TDR shows no large variations (figure 5.6). It proceeds on a quite stable level, disturbed by rain events. From middle of August on, the signal decreases and from October on increases slightly. In general *SM* by TDR shows a much smaller range than CRS and follows different respectively partly opposing pattern. Especially from middle of August to the middle of September a massive opposing trend in the signals of the TDR and the CRS is visible (figure 5.6). A growth-intensive stadium of fruit development may be the reason for this: a high root water uptake reduced soil moisture measured by the TDR near the trees (especially in the depths of the main root zone). The *SM* measured by CRS might be increased due to water storage in the biomass, caused by growth of the citrus fruit. An additional amount of water thus will be stored in the citrus fruit in the CRS footprint. During the time of moderate growth, trees have a mean water requirement of 26 % (compared to annual requirement), whereas during the time of intensive fruit expansion root uptake is about 40 % of the annual water requirement (Falivene et al., 2006). Obviously this may be the time when

the TDR signal decreases remarkably for one month. After the time of high water consumption and assumed fruit growth, soil moisture normalizes to a quite stable level due to the beginning stadium of fruit ripening and a stagnant amount of water stored in fruit.

Through the influence of the additional water pool, stored in citrus fruit, the CRS signal is distorted and needs a recalibration. After the assumed fruit growth stadium, it can be considered that the CRS does not show the actual soil moisture conditions on the orchard. Further research should be conducted to verify this hypothesis.

In general, values of TDR and CRS are not unfettered comparable because TDR measurements were made on a point scale whereas the CRS  $SM$  is a spatial integral. Due to the location of the TDR it is not representative for other locations and thus it misestimates areal mean  $SM$ . Besides this, the TDR does not measure  $SM$  directly just beneath the surface because the first sensor starts at five centimeters. Thus it underestimates the average  $SM$  between 0 and 5 cm. These restrictions will be conspicuous in the opposing values of  $SM$  between those two devices. On all scales CRS and TDR show a different variability in  $SM$ . A direct comparison between TDR and CRS can only be done using a distributed network which covers a large portion of the CRS footprint (as mentioned i.e. by Franz et al. (2012a) and Rivera Villarreyes et al. (2011)).

In the observed period,  $ET_a$  decreases and  $SM$  increases (figure 5.10). The reason of this development can be the same as mentioned above. With decreasing temperatures and insolation, soil moisture storage increases. From June to middle of September,  $ET_a$  and CRS  $SM$  follow partly similar fluctuations. An  $R^2$  of 0.15 shows only a weak correlation between the two factors. The peaks of the two components show however more or less similar characteristics which imply that conditions in the field are covered in a similar way by both footprints. Especially on a temporal mesoscale (weekly), a partly correlation can be observed. Mostly, an increase in  $SM$  leads to an increase in  $ET_a$ , caused by higher water availability for the plants. However, from middle of September onwards, the signals show obvious differences in their behavior. This difference started at the end of the assumed growth period of the citrus fruit which can be an indicator of a lack of a new calibration of the CRP (explained below). Especially in hot summer months (June to August) citrus trees partly suffer water stress accompanied by low CRS  $SM$  (figure 5.5 and 5.6) and TDR (particularly visible in the depth of 15 - 20 cm in figure 5.8). A large difference between the actual and potential evapotranspiration in July and August confirms that the citrus trees suffer from water stress, that leads to the lowest values of  $SM$ . Plants suffered water stress, the stomata of the plants might be predominantly weakly opened and only a small amount of water might transpire. Most of the time, variability of  $SM$  and  $ET_a$  is similar and they are influencing each other. However, there remain open questions concerning the behavior of the soil moisture, especially why it has such a big weekly dynamic.

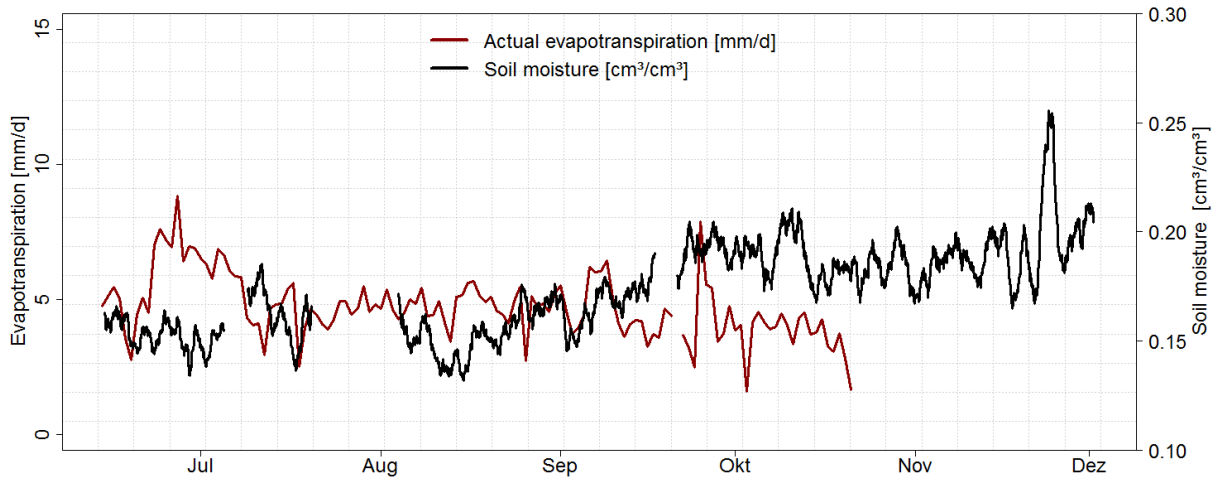


Figure 5.10: Relationship between CRS soil moisture and actual evapotranspiration.

The CRS  $SM$  was multiplied with the mean daily penetration depth of the CRS to convert it from  $\frac{cm^3}{cm^3}$  to  $mm$ . For the soil water balance, daily changes in the content of soil moisture were calculated (by subtracting midnight  $SM$  values). Franz et al. (2012a) used the daily mean value of the soil moisture but with this method an underestimation of the total flux can be engendered, thus this approach was not used here.

#### 5.2.4 Bottom Flux

As mentioned before, bottom flux describes the water movement in the soil-root-system and groundwater recharge or deep percolation water movement beneath the root zone, through the vadose zone to the ground water table. In the present study it was calculated after equation 3.1. Days without sufficient data (due to data gaps) for all components are not used in the calculation. Due to still remaining data for  $ET_a$ , measured by eddy covariance, the SWB could only be calculated until end of October. The total bottom flux for this time span was  $-140\ mm$ . It ranged from  $-6.6\ \frac{mm}{d}$  to  $6.7\ \frac{mm}{d}$  with a mean value of  $-1.35\ \frac{mm}{d}$ . Deep percolation, thus only the negative flux, made up an amount of  $-193\ mm$ .

Bottom flux is governed by gravity forces on water in the soil. It already occurs at small soil moisture contents, show high amounts around field capacity but reaches its maximum at saturation (negative values in figure 5.11). In the opposite direction capillary rise occurs and water moves upwards from the root zone (positive values in figure 5.11). In semi-arid regions only small rainfall occurs and thus only small deep percolation can contribute to the rise of groundwater table. As stated by Lepage (2012), natural recharge only occurs if monthly rainfall exceeds  $20\ mm$ . By excess irrigated agriculture (as on the present study) these values can be increased and an artificial recharge is induced.

Field capacity was not reached by integral CRS  $SM$  during the measurement period (figure 5.6). The optimal range of plant available soil water is between field capacity and the permanent wilting point, the so-called total available water (TAW). In the present study, the integral soil moisture ranges in between this margin. However, calculated percolation occurred quite often during the observed time span (figure 5.11). Since the  $SM$  is only an integral value of the whole footprint, it averages moist conditions near the dripper and dry conditions on the rows/roads. As mentioned before, dryer parts have a higher proportion on the orchard. It can be assumed that higher  $BF$  occurs near the dripper and minimal  $BF$  occurs at very dry conditions in the remaining areas. Thus the  $BF$  only occurs on a small fraction of the orchard. Altogether the bottom flux is more often negative than positive which is induced by the regular irrigation water surplus for leaching salination and thus deep percolation occurs.

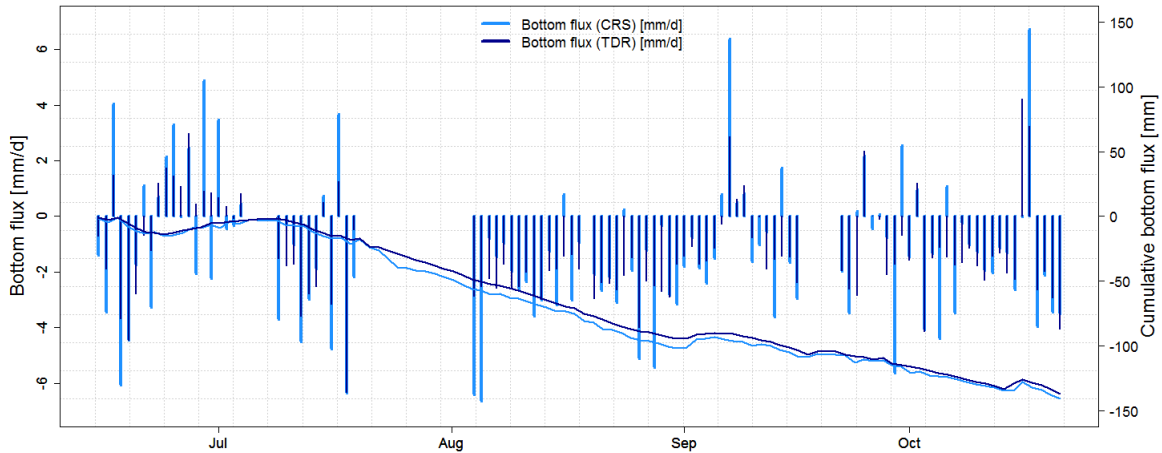


Figure 5.11: Bottom flux calculated by the SWB with two options of soil moisture storage change:  $SM$  of CRS (lightblue) and  $SM$  of TDR (darkblue). Additionally the cumulative bottom fluxes are shown.

If the SWB is calculated with the TDR  $SM$  only a slight difference of the bottom flux is visible (cumulative sums in figure 5.11). The TDR slightly underestimates the  $BF$  in comparison to the CRS. However, the results of the SWB are related to each other and show predominantly the same direction. Bottom flux by CRS  $SM$  is about 193 mm and by TDR  $SM$  168 mm for the observed time span. Daily differences in soil moisture storage changes (by CRS and TDR) are that small, that they do not have a high influence on the SWB. This slight difference in the results is a hint that the height of bottom flux is not governed mainly by soil moisture but rather by other influences.

In comparison the modification of the evapotranspiration at the SWB has a higher influence: the change from  $ET_a$  to  $ET_c$  leads to a stronger shift in the bottom flux (figure 5.12). Higher potential evapotranspiration (June to middle of August) leads to lower values in  $BF$  for the

observed time span. The cumulative sum of the  $BF$ , calculated with  $ET_c$ , is much lower than for the actual evapotranspiration because more water evapotranspirates and thus less water is available for  $BF$ . With this comparison the SWB shows a higher sensitivity to evapotranspiration than to soil moisture storage changes.

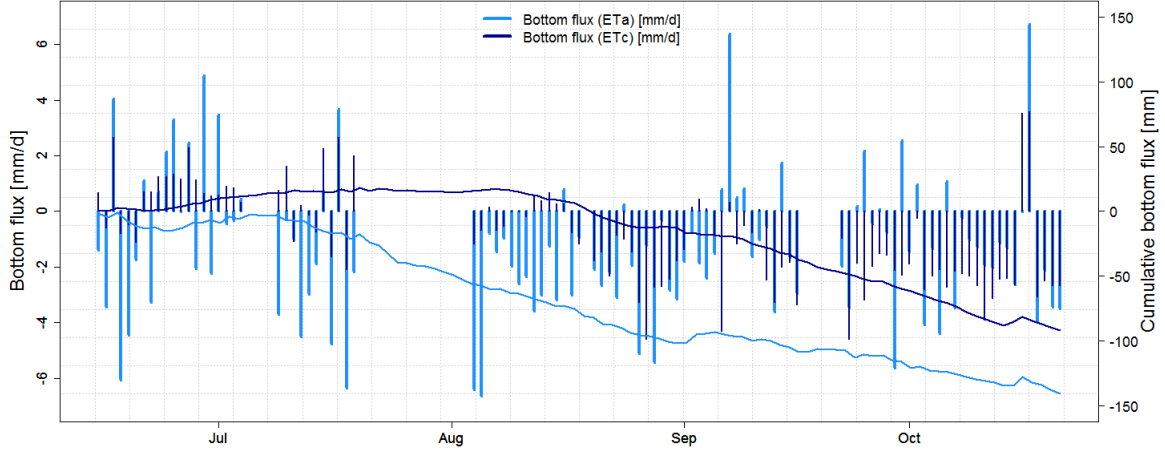


Figure 5.12: Bottom flux calculated with actual and reference evapotranspiration: bottom flux calculated with  $ET_a$  (lightblue) and  $ET_0$  (darkblue). Additional the cumulative bottom flux for both options is shown.

In order to validate the estimated  $BF$  calculated by the SWB, the comparison with the measured  $BF$  by fluxmeter has been done. For comparison there emerge problems due to the depths of the considered layers: the fluxmeter is installed on the surface and below the root zone (0 and 80 cm) and the SWB quantifies the  $BF$  in a shallower layer (0 - 15 cm). Due to the quite constant soil moisture conditions in the deeper layer below 60 cm (figure 5.8) it seems as if the fluxmeter underestimates the downward movement of water (appendix III). But the fluxmeter only measures a flux if saturated conditions in the soil prevail which happens quite rarely in a depth of 80 cm under semi-arid conditions and only after heavy rain events. The detector at the surface measured more often a flux than the detector in 80 cm depth. By root water uptake most of the water was transported to the trees and does not contribute any longer on the downward movement. Thus in the deep layers no saturated conditions prevail and no flux is measured. The fluxmeter detects a bottom flux of only 37 mm compared to the SWB with 193 mm for the investigated time span. Nevertheless the results of the SWB and the fluxmeter are also not unfettered comparable: the fluxmeter only gives information about the root zone of a citrus tree and the SWB uses integral components. Thus the fluxmeter gives a misestimating of spatial integral values.

The importance of the soil characteristics for water transport becomes clear by the sole infiltration event in 80 cm depth (fluxmeter): percolation induced by a heavy rain event in July (26

*mm*) was detected four days after the event (even if there was no infiltration water detected on the surface). This can be accounted to the low permeability of the loamy soil. As a consequence deep percolation proceeds slowly and needs longer for infiltration to reach deep layers. The deep percolation, measured in 80 cm depth by the fluxmeter is not comparable to the results of the SWB. The SWB only calculates deep percolation for the first 20 cm and thus it does not give any information about the soil layers below.

In a former study conducted on the present orchard Amenzou et al. (2013) determined a proportion of 37 % of the inflows as *DP*. In comparison to the present study the *DP* makes up a portion of 30 % of the inputs and thus is in the same range as in the mentioned study.

The weekly values of the balance are presented in table 5.3. For the calculation soil moisture values at midnight of the first and last day of the week were subtracted (even if values are not available for all days). The remaining components are summed up for the particular week. The highest values of deep percolation occur during the period with highest irrigation. But also the evapotranspiration shows a high influence: in week 26 highest *ET<sub>a</sub>* and just moderate irrigation lead to a positive bottom flux and thus plant water uptake was high and plant water stress occurred. Weeks of only little irrigation showed a small evapotranspiration and only small deep percolation. Thus a high relationship between these three components is visible.

Table 5.3: Weekly values of the soil water balance in [mm]. The direction of bottom flux is defined by the sign (negative for deep percolation and positive for water uptake).

calendar weeks	<i>P</i>	<i>I</i>	$\Delta S$ weekly	<i>ET<sub>a</sub></i>	<i>ET<sub>c</sub></i>	<i>BF</i> weekly
<b>25</b>	0.0	42.30	-3.38	32.13		-6.56
<b>26</b>	0.0	41.00	2.36	50.49		7.49
<b>27</b>	0.0	23.5	0.36	25.30		1.61
<b>28</b>	0.0	38.6	0.42	24.70		-14.15
<b>29</b>	0.0	30.3	-0.52	22.13		-7.46
<b>32</b>	0.0	49.40	0.18	33.27		-16.08
<b>33</b>	0.0	48.40	-3.46	33.99		-10.7
<b>34</b>	0.0	42.30	2.66	28.37		-11.49
<b>35</b>	0.0	50.00	-1.92	32.47		-15.37
<b>36</b>	0.80	36.10	0.97	34.58		-3.04
<b>37</b>	1.40	36.10	0.38	31.48		-6.17
<b>38</b>	16.40	38.5	1.36	23.23		-33.02
<b>39</b>	0.0	38.50	-1.25	31.52		-5.50
<b>40</b>	0.0	36.10	-1.42	26.88		-7.60
<b>41</b>	0.0	39.70	1.94	28.33		-13.11
<b>42</b>	0.20	28.60	-1.04	24.45		-3.13

The bottom flux is directly correlated to the single components of the SWB. The coefficient of determination shows different potential dependencies (table 5.4). The highest correlation shows

precipitation due to one very significant event in week 38 resulting in a high  $DP$ . There occurred more heavy rain events but due to lack of data support from CRS for this time, the SWB cannot be calculated for these events. Irrigation and actual evapotranspiration also show heightened correlation. Soil moisture shows only a low influence on the SWB on a weekly basis. In general it can be stated, that irrigation and evapotranspiration have the highest influences (additional shown by figure 5.12 and the irrigation modeling in section 5.3) to the bottom flux.

Table 5.4: Coefficient of determination for the relationship of bottom flux and the single components (precipitation, irrigation, actual evapotranspiration and soil moisture storage changes) of the SWB.

$BF\$$	$R^2$ _ weekly
$P$	0.4897
$I$	0.156
$ET_a$	0.2194
$\Delta S$	0.0003

Most of time, irrigation is overdesigned and a remarkable amount of water percolates downwards. Not only the amount of irrigation but rather its timing can be an important parameter to govern  $BF$ . In semi-arid systems it is important to keep the golden mean between efficient irrigation, salt leaching and irrigation water recharge. For having a better understanding of the behavior of the orchard as a hydrological unit, a water management modeling was done and is explained in the following section.

### 5.3 Water Management Modeling

As shown in the last section, irrigation is a sensitive parameter for the dimensioning of deep percolation. It is the sole compartment of the SWB which can be regulated by the farmer and thus it can pointedly govern the  $DP$ . In semi-arid systems it is important to choose the best way in water management: on the one hand minimum irrigation with highest efficiency is practical to save water. On the other hand application of high irrigation contributes to groundwater recharge. Which way of irrigation is chosen depends on the status of the water resources in the basin (are surficial and groundwater resources scarce?) and the aim of irrigation (having the best cost-efficiency-relation or contribute to groundwater recharge?). With the WatBal model the simulation of different irrigation approaches on the present orchard was possible. Those approaches were investigated and evaluated for their suitability on groundwater recharge or water saving (appendix IV).

For a reproduction of results that fit conditions on the orchard, a validation of the model was done. For this aim, two options were possible: to use TDR  $SM$  or to use CRS  $SM$  as validation parameter. In the present modeling, CRS  $SM$  was used. The TDR only gives point information

and does not show general conditions on the orchard with its heterogeneous conditions at *dripper*, *trees* and *rows*. Temperature, precipitation, relative humidity, wind speed and net radiation measured on the orchard are inserted as meteorological input parameters to the model. By equation 3.12 the reference evapotranspiration was calculated. Crop parameters for the three growth stadia (initial, middle, end) were adjusted to citrus trees with a  $K_c$  of 0.6, a root depth of 40 cm and a leaf area index of 4.5, 4.5 and 3.7 for the three periods. Loamy soil was chosen in the soil options with values of 0.26  $\frac{\text{cm}^3}{\text{cm}^3}$  and 0.12  $\frac{\text{cm}^3}{\text{cm}^3}$  for field capacity and wilting point and given 59 mm as initial soil moisture.

Due to the irregular distribution of dry (30 %) and moist areas (70 %) in the footprint, modelling included both conditions. For dry conditions, a scenario with one third<sup>4</sup> of the irrigation amount, applied on the orchard, and with a low initial soil moisture (5 mm) was calculated. For moist conditions, the scenario was calculated with full irrigation (as applied on the orchard) and the initial water content given by the model (59 mm). Resulting  $SM$  was weighted for the proportions of the areas on the orchard. Weighted soil moisture shows a behavior, partly comparable to the conditions on the orchard. It has a quite stable course of soil moisture which increases in the late autumn, as  $SM$  of CRS. Nevertheless, the range of the WatBal  $SM$  is much smaller and also the increase distinct flatter (figure 5.13). Particularly the steep increase of CRS  $SM$  from August to September is not displayed by WatBal. This can be an additional confirmation that the CRS  $SM$  increase is not induced by meteorological conditions but rather by the growth of the citrus fruit. Altogether it is ascertainable that the model gives an approximate reproduction of the reality without being an exact representation of real conditions on the orchard.

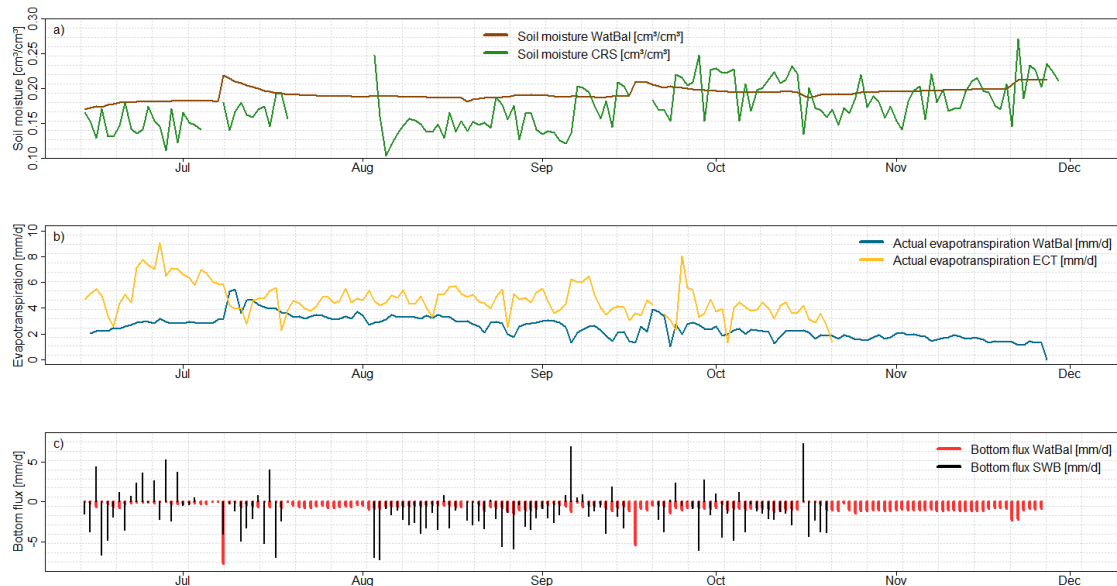


Figure 5.13: Comparison of modelled and calculated values of  $SM$ ,  $ETa$  and  $DP$ .

<sup>4</sup>The irrigation was set to  $\frac{1}{3}$  of the original irrigation amount of the orchard because even on dry areas the irrigation has an effect due to water movement in the soil or surficial runoff.

Actual evapotranspiration also was simulated for the dry and wet scenarios, weighted afterwards and compared to ECT  $ET_a$ . However, the model does not reproduce fluctuations that well and in general it underestimates  $ET_a$  (figure 5.13). These differences may result from the distinction between modelling with data of point measurements ( $ET_0$ ) in comparison to the ECT measurements on field scale. Same results and reasons can be stated for the bottom flux. Furthermore, a high proportion of dry areas was used for the validation-weighting of  $SM$ . This fraction might be too high and thus tit results in these underestimations.

With the knowledge of well model reliability, different irrigation scenarios were applied. The results for  $DP$  of the different approaches were weighted for the same portions as the validation data set (30 % of moist areas and 70 % of dry areas).

When using **automatic irrigation** the application of water is controlled by the efficiency and the threshold when irrigation starts. Two approaches were modelled, for both an efficiency of 0.8 was chosen because it is a typical value for drip irrigation and thus reproduces better the conditions in the field (table 5.5). The two approaches were distinguished by their threshold ( $\alpha$ ). It can be chosen from zero to two and was altered here from 0.2 to 0.8. With the lowest threshold (0.2) a constant irrigation every second day was applied. With a threshold of 0.8, only sparse irrigation was calculated with high irrigation amounts for each irrigation. Automatic irrigation leads to small amounts of deep percolation but to high total irrigation water amounts in opposite to the present conducted irrigation practice on the orchard. Soil moisture mostly has a large variability between the critical point (beneath this point, plants suffer water stress) and field capacity. This implies close-to-stress conditions for the plants. The application of daily irrigation amounts of around 10 - 15 mm is physically not possible for drip irrigation, thus this irrigation approach is partly not feasible on the present orchard.

For modelling the **irrigation by sprinkler** the threshold of water availability( $\alpha$ ), the mean amount of irrigation water ( $I$ ) und the irrigation intervals ( $d$ ) have to be chosen. First, the frequency was set to daily; the irrigation amount was set to 5.5 mm (mean irrigation amount on the orchard) and the threshold was altered between 0.2 and 0.8. By the choice of such a low irrigation height, the delivery method has switched to drip irrigation. Sprinkler systems have to irrigate higher amounts of water, otherwise their efficiency decreases and a high amount of irrigated water evaporates directly from the soil. Constant daily irrigation for the first weeks (June to August) and scarcer irrigation for the remaining weeks was the result. Deep percolation zero under given settings and the soil moisture conditions are held quite stable between field capacity and critical point. By changing the frequency to an interval higher than one, e.g. two to four days the height of the irrigation was increased to match plant water demands. For irrigation heights smaller than 15 mm per irrigation, plants suffer water stress and thus the irrigation should not undercut this height. However, by this method high irrigation amounts are applied. And thus the delivery method has to be switched back to sprinkler, because it is not

feasible for drip irrigation to deliver such high daily amounts. Deep percolation was zero for all approaches, thus the sprinkler (respectively drip) irrigation has the highest effectivity concerning the prevention of deep percolation.

In summary, it can be stated that the height of irrigation mainly should be adjusted to the water management plan of the considered orchard. In the present study the recharge of the groundwater should be induced by irrigation on the citrus orchard. Thus the actual irrigation practice delivers best results because it produces the highest values of deep percolation. Compared to this approach the modelled scenarios all result in a lower  $DP$ . However, if the aim of irrigation is a high effectivity and saving as much water as possible, one of the modelled approaches fits better. Sprinkler irrigation with a low threshold and a high efficiency achieve smallest percolation amounts and thus most of the water is used directly by the plants. Though with this approach no salt leaching is possible and the danger of salinization of the soil is given. Approaches which lead to low  $DP$  rates are not applicable on the present orchard because salt leaching is needed.

Table 5.5: Results of irrigation modelling from the WatBal model. The irrigation, conducted on the present orchard was compared to automatic and sprinkler irrigation approaches.

	Parameter	# Irr	Irr [mm]	DP [mm]
Original		167	499	125
Automatic I	$\alpha=0.2, \eta=0.8$	56	380	10
Automatic II	$\alpha=0.8, \eta=0.8$	19	388	23
Sprinkler I	$\alpha=0.2, I= 5.5, d=1$	104	376	7
Sprinkler II	$\alpha=0.8, I=5.5, d=1$	96	363	0
Sprinkler III	$\alpha=0.8. I=5.5, d=2$	70	320	0
Sprinkler IV	$\alpha=0.8. I=10, d=2$	53	362	0



# 6 Discussion

## 6.1 Assessment of Irrigation Recharge

On the present orchard, irrigation has the aim to ensure plant water demands and providing groundwater recharge. As a result of the previous calculations, one third of irrigation and precipitation ( $638\text{ mm}$ ) move as deep percolation ( $193\text{ mm}$ ) through the root zone to the aquifer. The precision of this value is the result of the accuracy of the single SWB components. By the combination of eddy covariance technique and cosmic ray sensing a quite good impression of the processes on the field scale were given. However, they give a mean value for conditions in the field which can be problematic due to the mentioned heterogeneities: especially in the tree lines higher soil moisture coupled with higher evapotranspiration are present. It is also expectable that the major amount of deep percolation occurs directly beneath the drip irrigation. On areas with missing irrigation or vegetation, soil moisture is that low that no deep percolation is expected. Thus the resulting values cannot be seen as representative for all areas on the orchard.

During the time of measurement, CRS had a mean penetration depth of around 15 cm. Thus mean soil moisture storage is calculated for the soil layers of 0 - 15 cm. However, soil water movement also takes place in depths, deeper than this considered depths. Notably interactions among plants, soil and root water occur and thus these changes in water content are not gathered by CRS. It can be preceded on the assumption that storage changes measured by CRS underestimate the processes occurring in layers, deeper than 15 cm. By having additional TDR sensors which cover the horizontal heterogeneities on the orchard, soil moisture storage changes might be captured or complemented better in those depths.

A validation of the resulting deep percolation was not possible in detail: the installed fluxmeter has a quite insensitive detection level because it only measures a deep percolation for saturated conditions in the soil. It underestimates the movement of the soil water drastically and thus it is not used for comparison here. The modeling with the WatBal sheet also showed non-satisfactory results: due to a quite uncertain model validation, a supposed general underestimation of deep percolation occurred. In comparison to a former study of Amenzou et al. (2013) on the present orchard, the deep percolation is in the same range as calculated here.

The calculated deep percolation will contribute to groundwater recharge in the aquifer system of the Haouz plain. Due to a deep groundwater table beneath the orchard and a fine textured soil, water movement through the vadose zone towards the groundwater table can take long. The

quantification of water movement through the vadose zone might be done by a computer model for groundwater flow. The results can be used for a better estimation of the yearly groundwater recharge.

The utilization of irrigation water for groundwater recharge is only efficient if irrigation water is not delivered by groundwater pumping. In the present study, mainly surface water from the Lalla Takerkoust reservoir is used for irrigation water delivery and thus groundwater recharge is quite effective. However, only small daily amounts of *DP* from the orchard, referred to the aquifer extent, contribute to the recharge and thus the effectivity of the recharge is dubiously. A more forceful groundwater recharge can be achieved by the use of infiltration basins or canals and by specific drainage wells.

The SWB shows highest sensitivity to irrigation and evapotranspiration. The WatBal modeling showed that irrigation height and time have a high influence on the downward percolating water. Even if absolute values of deep percolation are apparently underestimated, general processes and direction of water movement are reproduced well. Irrigation is the only one which can be influenced by the farmer. Thus its careful management and timing is an essential task to govern the ground water recharge. Management always should consider the source of irrigation water. If groundwater is used in a region with groundwater scarcity and no surface water resources, than an approach with the highest efficiency should be used. However, in the present case, when a region with groundwater scarcity commands sufficient surface water resources, then the approach of irrigation recharge can be realized.

## 6.2 Applicability of CRS on heterogeneous Soil Conditions

In the actual study, the application of cosmic ray sensing on an irrigated orchard was conducted. Due to the vertical and horizontal heterogeneous soil moisture distribution on the orchard, a weighting function for the calibration was necessary. The common calibration approach after Desilets et al. (2010) does not take any heterogeneities in the footprint into account. However, Franz et al. (2013a) mentioned that neutron counts depend on the spatial structure of the soil moisture in the footprint. Thus calibration procedure was modified by spatial and vertical weighting of the calibration data set. This process lead to a lower average soil moisture with smaller fluctuations. Due to stable climatic and hydrologic conditions and the larger proportion of dry areas to the total area, it can be assumed that weighted soil moisture gives a better idea of the real conditions. However, the quality of the calibration soil data set was diminished due to unfavorable conditions while soil sampling. The stony, loamy soil lead quite often to disturbed soil cores which made it difficult to reproduce authentic bulk density and soil moisture for calibration. Moreover due to high temperatures and material fatigue only 16 instead of 18 points were sampled which made an averaging from the beginning difficult. A calibration after Franz et al. (2013a) might have been a better way for the determination of a calibration

data set. This approach is unaffected by stones, cobbles and such unfavorable conditions as occurred on the orchard. However, for this calibration approach a higher effort for analysis of the chemical composition of the soil is needed. However, this analysis was not possible under given conditions. As recommended by Baatz et al. (2014), universal calibration approach or the calibration by COSMIC do not induce as large fluctuations in the neutron intensity as the here chosen approach. Maybe by choosing another calibration approach the variability of the CRS signal on intermediate temporal scale might be reduced under present conditions.

The applicability of CRS for short- and long-time measurements (daily to seasonal) was one main question to investigate. The analysis of the temporal variability of CRS showed different results. On the daily scale the variation of soil moisture, induced by irrigations and evapotranspiration, is vaguely informative. Only a slight mean variability in the day makes the distinction of the six daily irrigation events difficult and not obvious. In detailed consideration of single days the diurnal run of the soil moisture is not reproduced satisfactorily. The mentioned heterogeneous soil moisture conditions and the coverage of different irrigation sectors by the footprint can be the reason for the inconclusive signal. Dry and unirrigated areas represent the majority of the area on the orchard. These areas have stable soil moisture conditions on a quite low level and a big influence to the footprint. Thus the smaller proportion of irrigated areas does not have that big influence on the footprint and thus daily variability of CRS *SM* is in average small.

Weekly resolution did not show a clear pattern. Especially under given stable conditions, fluctuations do not show a certain consistence. From June to middle of September, soil moisture partly follows same fluctuations as actual evapotranspiration. These components influence each other and it can be assumed that their variability is governed by vegetative influences of the citrus trees. A more detailed analysis of the influence of transpiration habits to these two components could be done by a sap flow determination, as investigated by Er-Raki et al. (2009). Fluctuations of neutron intensity on daily and weekly scale might be induced by relatively low neutron counts on the site and a high amount of biomass. Those two factors can decrease the accuracy of the neutron counts and increase the noise in the signal (Baatz et al., 2014).

Evaluating the whole time series, three significant periods of *SM* are distinguishable: from June to middle of August stable but low soil moisture conditions occurred. From middle of August to mid-september a steep increase of soil moisture over one month leads to stable and general moister conditions after this time. In the first and third period, soil moisture is fluctuating around a quite constant level. As mentioned before, with the existing data these weekly fluctuations are not understood and thus cannot be explained here. The steep increase can be an indicator for a change in vegetation. In the time of increasing soil moisture, citrus fruit might have experienced their main growth and thus a large additional amount of water was stored in the footprint of the CRP. In comparison to the *SM* of TDR this assumption can be confirmed. Due to a calibration for conditions without citrus fruit, soil moisture measurement of the CRP resulted after the

growth period to a higher average value. From this fact it is apparent that a recalibration for the conditions after middle of September is needed to gain realistic *SM* values.

With a well-equipped distributed sensor network, as described in Rivera Villarreyes (2014), the increase in vegetation can be quantified without an additional calibration. Using the relation between expected (soil moisture of TDR) and measured (soil moisture of CRS) neutrons, an accumulation in biomass can be determined. Since there is no sensor network or representative distributed TDRs on the present orchard, it was not possible to use this approach.

Therefore it has to be assumed that the measured CRS soil moisture, especially after its steep rise does not reproduce the conditions in the field. The validation of the WatBal model showed a confirmation of these assumptions: in the model *SM* increased consistently in time of investigation. Since the model calculates the expected *SM* by the climatically and vegetative information given to the model, such a steep rise of soil moisture was not calculated.

A further validation of the CRS signal was not possible because a well-equipped distributed sensor network did not exist on the orchard. The sole TDR, installed beneath a citrus tree, only gave point information for one specific location on the orchard. TDR *SM* showed a different behaviour than CRS *SM* on all temporal scales and thus it cannot be used for validation. As described by Franz et al. (2013a), with increasing size of heterogeneous soil moisture areas in the footprint, the placement of the detector in the field will become more sensitive to small-scale conditions. In the present study the opposing soil moisture fields do not exceed a distance of 10 m (as mentioned by Franz et al. (2013a)) in the planted fields but on the larger agricultural roads. They make up an amount of 10 % of the total area in the footprint. Thus for future investigations it should be examined whether the placement of the CRP on an orchard with given conditions is sensitive to those different spots.

Due to 20 days of data gaps which partly occurred during the heaviest rain events, information about the behavior of CRS under those special hydrologic conditions were missed.

### 6.3 Soil Water Balance on Field Scale

By combination of cosmic ray sensing and eddy covariance technique the accuracy of the soil water balance was increased. It can be stated that the footprints of both techniques are compatible and cover more or less same areas. Under given hydrological and climatically conditions sizes of the footprints can have a high influence to the fitting of the *SM* and *ET<sub>a</sub>* signals. The larger the area of the footprint, the larger the influence of dry areas (from the orchard itself and surrounding areas). Dry areas only have little partition to the actual evapotranspiration and thus *ET<sub>a</sub>* will be smaller. If footprint size is very small, irrigated areas can have higher influences. Thus not fitting footprint sizes can result in misestimating of water fluxes. In the present study interacting soil moisture and actual evapotranspiration show partly a common variability, especially until September. After middle of September, the assumed end of citrus fruit growth period, behaviors

of  $SM$  and  $ET_a$  are divergent. This difference can be due to the mentioned changes in behavior of the soil moisture after this time. Unfortunately the investigations are limited to a part of the observed period because not full data supply for the eddy covariance data was available. With a longer time series of  $ET_a$ , the assessment of a combination of these two techniques could have been more precise.

## 6.4 Outlook

Following studies on the orchard should focus on the validation of the single components of the soil water balance. Especially a better validation of deep percolation by more detailed measurement setups (e.g., lysimeter) can increase the reliability of the presented results. This investigation has the highest priority because its quantification was the aim of the present study. With a better equipped sensor network, soil moisture derived from neutron intensity might be evaluated better to the heterogeneous and changing conditions.

An additional calibration can validate or correct the assessment of a change in biomass. By renewed CRS investigations on a comparable or same orchard, a longer time period should be covered to detect the reaction of neutron intensity to the different growth stage of citrus trees or their management steps. Due to the relative short measurement period of nearly half a year, important changings in the CRS signal like pruning of the trees or the harvest of the fruit were missed. It would be interesting whether a leap in the signal after harvest occurred, back to biomass conditions during calibration. However, by organizational reasons this was not possible in the actual investigation.

A better understanding of the weekly dynamics is important for future investigations. Especially under given conditions, the transpiration of the biomass and its influence to the neutron intensity should be investigated. Actual researches are not known for semi-arid irrigation conditions and thus this is still an open field.

Under given vegetative conditions, it is conceivably to quantify the accumulation of biomass as an economically working knowledge. In the present study, a decrease in neutron intensity might be mainly induced by the growth of citrus fruit. Changes in other biomass components can be excluded by slow growth of citrus trees and regular pruning. By knowing the changes in soil moisture (by comparison with other sensors) during the measurement and knowing the contained water in a fully grown citrus fruit (values taken by literature), the agricultural and economical yield of a vegetation period might be estimated. This knowledge could be used by the farmer to have a detailed assessment of the expected yield. This method especially may be used on large or far afield located orchards.

In general the investigations imply that an application of cosmic ray sensing for irrigated semi-arid agriculture is possible. With further improvements of the calibration procedure by multiple calibration data sets or a MCNPx modeling in combination with local site conditions, improved

results of the soil moisture conditions on the orchard are expectable.

Values of groundwater recharge, induced by the irrigation on the orchard, can be implemented in the modeling of the decision support system, developed by Lepage (2012). It gives more detailed information about soil moisture than results of remote sensing or point measurements and thus can be used for validation or extension of the groundwater model.

## Conclusion

The assessment of the irrigation recharge for the Haouz aquifer beneath an irrigated citrus orchard southwest of Marrakesh (Morocco) was the aim of the present work. For its quantification a soil water balance was set up on field-scale. The combination of the eddy covariance technology and the cosmic ray sensing led to a higher accuracy than upscaling from point measurements due to the larger footprint of the technologies which integrate the occurring heterogeneities. Resulting from an investigation of six month (June to December 2013) an irrigation recharge of one third of the input amounts (irrigation and precipitation) was calculated. Thus it can be stated that besides a sufficient salt leaching also groundwater recharge occurs. A validation of these results was not possible due to lacking reference data of spatial deep percolation. A fluxmeter, installed on the orchard, gave point information but it measures percolation only for saturated soil conditions and thus it was not applicable for validation. For future work it is urgently important to validate the measured deep percolation to use its results for policy and decision making.

The combination of the two field-scale measurements gave a good impression of interacting evapotranspiration and soil moisture on the orchard. The combined technologies are well applicable for field-scale measurements under given hydrological and climatical conditions.

Due to irrigation, the orchard possesses areas of moist to saturated conditions (around the dripper) and areas with drier conditions (beneath and between the trees). Since cosmic ray sensing gives an integral value for the soil moisture in its footprint, it imposes weighting of the calibration data set for heterogeneous soil moisture conditions. This was also described by Franz et al. (2012a) who developed a depth weighting function. Spatial and vertical weighting result in a lower average soil moisture with smaller fluctuations and these smoothed values describe the conditions in the field distinctly better. This result confirms that a weighting of the calibration data set is required if notable heterogeneities occur in the footprint of the cosmic ray probe. Weekly fluctuations in neutron intensity are high for given stable hydrological conditions and not well explainable with the given information. A steep shift of soil moisture in late summer will be assumed as accumulated water in citrus fruits. Missing data of validation made a verification of this assumption vague. By a recalibration after this period and additional phenological information this behavior could be understood.

Thus in future investigations the transpiration behaviour and growth periods of citrus trees and the sensitivity of the probe to the spatial heterogeneities should be better understood to explain the variations in the measured soil moisture. A validation of the integral soil moisture with point-measurements from a TDR leads to non-satisfactory results. Thus under given conditions a thorough validation of the cosmic ray neutron intensity is necessary.

The present study shows remaining uncertainties for the application of cosmic ray sensing under given climatical and agricultural conditions. Nevertheless the methodology is promising

for the resolving of current and future problems of water management. By further research and investigations a better validation of the results can be achieved. That opens and enhances the possibilities of the usage of the CRS technology not only for the research, but also for the agriculture and the urban and rural water supply.

# Bibliography

- Abtew, W., Melesse, A., 2013. Evaporation and Evapotranspiration: Measurements and Estimations. Springer, Berlin and Heidelberg.
- Allen, R., 1998. FAO Irrigation and Drainage Paper: No. 56. Rome.
- Amenzou, N., Marah, H., Raibi, F., Ezzahar, J., Khabba, S., Lionel, J., Ismaili, M., 2013. Estimation of soil evaporation and infiltration losses using stable isotope, fluxmeter and Eddy-Covariance system for Citrus Orchards in a semi-arid region (Morocco). Academia Journal of Environmental Sciences (1), 001–008.
- Aubinet, M., Vesala, T., Papale, D., 2012. Eddy Covariance: A Practical Guide to Measurement and Data Analysis. Springer, Berlin and Heidelberg.
- Baatz, R., Bogena, H., Hendricks Franssen, H.-J., Huisman, J., Qu, W., Montzka, C., Vereecken, H., 2014. Calibration of a catchment scale cosmic-ray probe network: A comparison of three parameterization methods. Journal of Hydrology.
- Baroni, G., Gandolfi, C., 2009. User manual of the spreadsheet Water balance with FAO – Penman Monteith method v.2.0.
- Blume, H.-P., Stahr, K., Leinweber, P., 2011. Bodenkundliches Praktikum: Eine Einführung in pedologisches Arbeiten für Ökologen, insbesondere Land- und Forstwirte, und für Geowissenschaftler, 3rd Edition. Spektrum Akademischer Verlag, Heidelberg.
- Bogena, H. R., Huisman, J. A., Baatz, R., Hendricks Franssen, H.-J., Vereecken, H., 2013. Accuracy of the cosmic-ray soil water content probe in humid forest ecosystems: The worst case scenario. Water Resources Research 49 (9), 5778–5791.
- Bundesanstalt für Geowissenschaften und Rohstoffe, 2006. Bodenkundliche Kartieranleitung. 5. verbesserte und erweiterte Auflage. Schweizerbart'sche Verlagsbuchhandlung, Stuttgart.
- Burba, G., 2013. Eddy Covariance Method: for Scientific, Industrial, Agricultural and Regulatory Applications. Lincoln and Nebraska.
- Chehbouni, A., Escadafal, R., Duchemin, B., Boulet, G., Simonneaux, V., Dedieu, G., Mougenot, B., Khabba, S., 2008. An integrated modelling and remote sensing approach for hydrological

- study in arid and semi-arid regions: the SUDMED Programme. *International Journal of Remote Sensing* 29 (1), 5161–5181.
- Desilets, D., Zreda, M., Ferré, T. P. A., 2010. Nature's neutron probe: Land surface hydrology at an elusive scale with cosmic rays. *Water Resources Research* 46 (11), 1–7.
- Deutscher Wetterdienst, 2013. Climate data of airport Marrakesch, Menara: Climate data of airport Marrakesch, Menara.
- URL [www.dwd.de](http://www.dwd.de)
- Dyck, S., Peschke, G., 1983. *Grundlagen der Hydrologie*. Ernst Klett, Berlin.
- Er-Raki, S., ???? Estimation des Besoins en eau des cultures.
- Er-Raki, S., Chehbouni, A., Ezzahar, J., Khabba, S., Boulet, G., Hanich, L., Williams, D., 2009. Evapotranspiration Partitioning from Sap Flow and Eddy Covariance Techniques for Olive Orchards in Semi-Arid Region. *Acta Hort* (846).
- Er-Raki, S., Ezzahar, J., Hanich, L., 2012. Evaluation of the Sap Flow Measurements Determined with Heat Balance Method for Citrus Orchards in Semi-Arid Region. *Acta Horticultural* (951), 259–268.
- Evett, S. R., Howell, T. A., Steiner, J., Cresap, J., 1993. Evapotranspiration by Soil Water Balance using TDR and Neutron Scattering. Proceedings of the National Conference on Irrigation and Drainage Engineering, 914–921.
- Falivene, S., Giddings, J., Hardy, S., Sanderson, G., 2006. Managing citrus orchards with less water. *Primefact* (427).
- Foken, T., 2006. *Angewandte Meteorologie: Mikrometeorologische Methoden*, 2nd Edition. Springer, Berlin and Heidelberg.
- Franz, T. E., Zreda, M., Ferre, T. P. A., Rosolem, R., 2013a. An assessment of the effect of horizontal soil moisture heterogeneity on the area-average measurement of cosmic-ray neutrons. *Water Resources Research* 49 (10), 6450–6458.
- Franz, T. E., Zreda, M., Ferre, T. P. A., Rosolem, R., Zweck, C., Stillman, S., Zeng, X., Shuttleworth, W. J., 2012a. Measurement depth of the cosmic ray soil moisture probe affected by hydrogen from various sources. *Water Resources Research* 48 (8), 1–9.
- Franz, T. E., Zreda, M., Rosolem, R., Ferre, T., 2012b. Field Validation of a Cosmic-Ray Neutron Sensor Using a Distributed Sensor Network. *Vadose Zone Journal* 11 (4).
- Franz, T. E., Zreda, M., Rosolem, R., Ferre, T. P. A., 2013b. A universal calibration function for determination of soil moisture with cosmic-ray neutrons. *Hydrology and Earth System Sciences* 17 (2), 453–460.

## Bibliography

---

- Glendon, W. G., Hillel, D., 1988. Groundwater recharge in arid regions: Review and critique of estimation methods. *Hydrological Processes* 2, 259–266.
- Güntner, A., Creutzfeldt, B., Dill, D., Barthelmes, F., 2012. Die Variabilität des kontinentalen Wasserkreislaufs in GRACE-Schwerefelddaten. *System Erde* 2 (1), 26–31.
- Hillel, D., 1998. Introduction to environmental soil physics. Elsevier Acad. Press, Amsterdam.
- Huang, P. M., Li, Y., Sumner, M. E., 2011. Handbook of soil sciences, 2nd Edition. CRC and Taylor & Francis, London.
- Kodama, M., Kudo, S., Kosuge, T., 1985. Application of atmospheric neutrons to soil moisture measurement. *Soil Science* (140), 237–242.
- Koo, R. C. J., 1961. The Distribution and Uptake of Soil Moisture in Citrus Orchards. Florida Agricultural Experiment Stations Journal Series (1360).
- Leibundgut, C., Maloszewski, P., Kulls, C., 2009. Tracers in Hydrology, 1st Edition. John Wiley & Sons Ltd.
- Lepage, M. e., 2012. An Integrated DSS for Groundwater Management Based on Remote Sensing. The Case of a Semi-arid Aquifer in Morocco. *Water Resources Management* 26 (11), 3209–3230.
- Limam, N., unknown. Perspectives de développement des ressources en eau dans le bassin du tensift.
- Michard, A., 2008. Continental evolution: The geology of Morocco: Structure, stratigraphy and tectonics of the Africa-Atlantic-Mediterranean triple junction. Vol. 116 of Lecture notes in earth sciences. Springer, Berlin and London.
- Müller-Hohenstein, K., Popp, H., 1990. Marokko: Ein islamisches Entwicklungsland mit kolonialer Vergangenheit, 1st Edition. Länderprofile, geographische Strukturen, Daten, Entwicklungen. Ernst Klett, Stuttgart.
- Neutron Monitor Database, 2013. Neutron monitor in Castilla la Mancha.  
URL <http://www.nmdb.eu/>
- Newman, H., 2012. Citrus irrigation recommendations: Farmnote 544. South Perth.
- Rivera Villarreyes, C., 2014. Cosmic-ray neutron sensing for soil moisture measurements in cropped fields. Ph.D. thesis, University of Potsdam, Potsdam.
- Rivera Villarreyes, C. A., Baroni, G., Oswald, S. E., 2011. Integral quantification of seasonal soil moisture changes in farmland by cosmic-ray neutrons. *Hydrology and Earth System Sciences* 15 (12), 3843–3859.

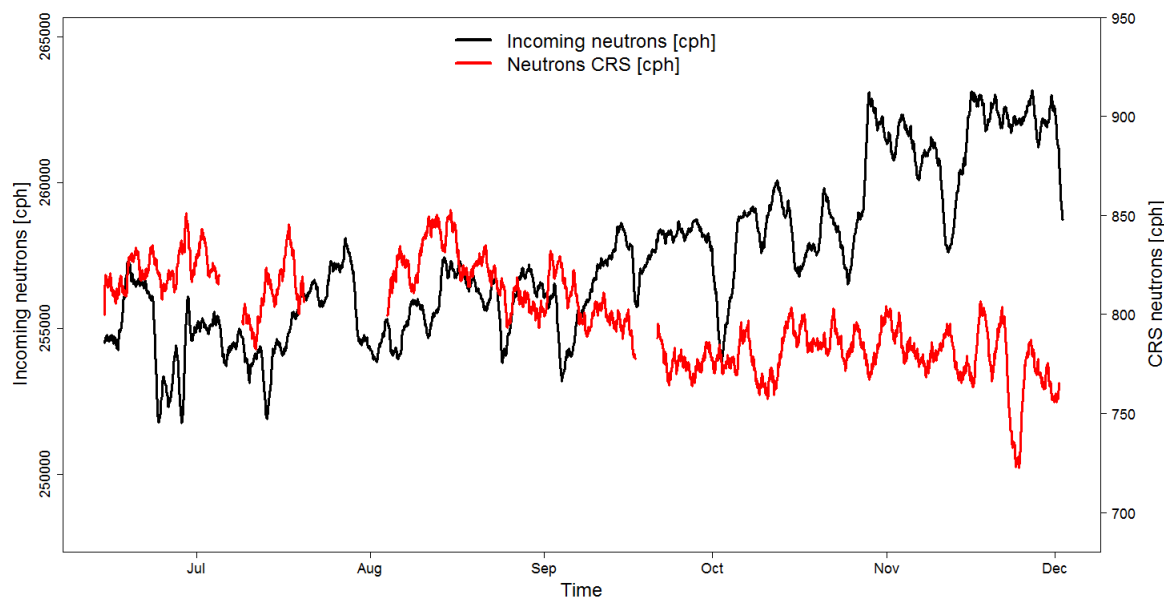
## Bibliography

---

- Rosolem, R., Shuttleworth, W. J., Zreda, M., Franz, T. E., Zeng, X., Kurc, S. A., 2013. The Effect of Atmospheric Water Vapor on Neutron Count in the Cosmic-Ray Soil Moisture Observing System. *Journal of Hydrometeorology* (14), 1659–1671.
- Royaume du Maroc, 2005. Recensement général de la population et de l'habitat de 2004: Population légale du Maroc.
- Schlickeiser, R., 2002. *Cosmic Ray Astrophysics. Astronomy and Astrophysics Library*. Springer, Berlin and Heidelberg.
- Shuttleworth, J., Rosolem, R., Zreda, M., Franz, T., 2013. The COsmic-ray Soil Moisture Interaction Code (COSMIC) for use in data assimilation. *Hydrology and Earth System Sciences Discussions* 10 (1), 1097–1125.
- United Nations Environment Programme, 2008. *Freshwater Under Threat: Vulnerability Assessment of Freshwater Resources to Environmental Change: Africa*.
- Vereecken, H., Huisman, J., Pachepsky, Y., Montzka, C., van der Kruk, J., Bogena, H., Weihermüller, L., Herbst, M., Martinez, G., Vanderborght, J., 2013. On the spatio-temporal dynamics of soil moisture at the field scale. *Journal of Hydrology*.
- Wirtschaftskammer Österreich, 2013. Länderreport Marokko.
- Zreda, M., Desilets, D., Ferré, T. P. A., Scott, R., 2008. Measuring soil moisture content non-invasively at intermediate spatial scale using cosmic-ray neutrons. *Geophysical Research Letters* 35 (21).
- Zreda, M., Shuttleworth, W. J., Zeng, X., Zweck, C., Desilets, D., Franz, T., Rosolem, R., 2012. COSMOS: the COsmic-ray Soil Moisture Observing System. *Hydrology and Earth System Sciences* 16 (11), 4079–4099.

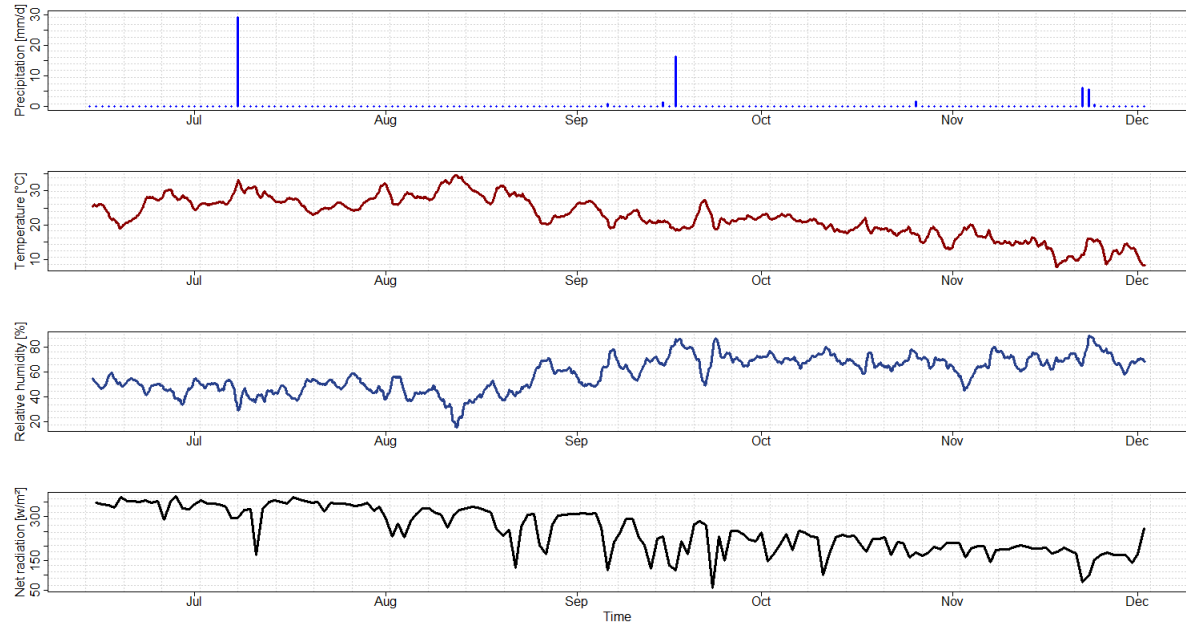
# Appendix

## Appendix I



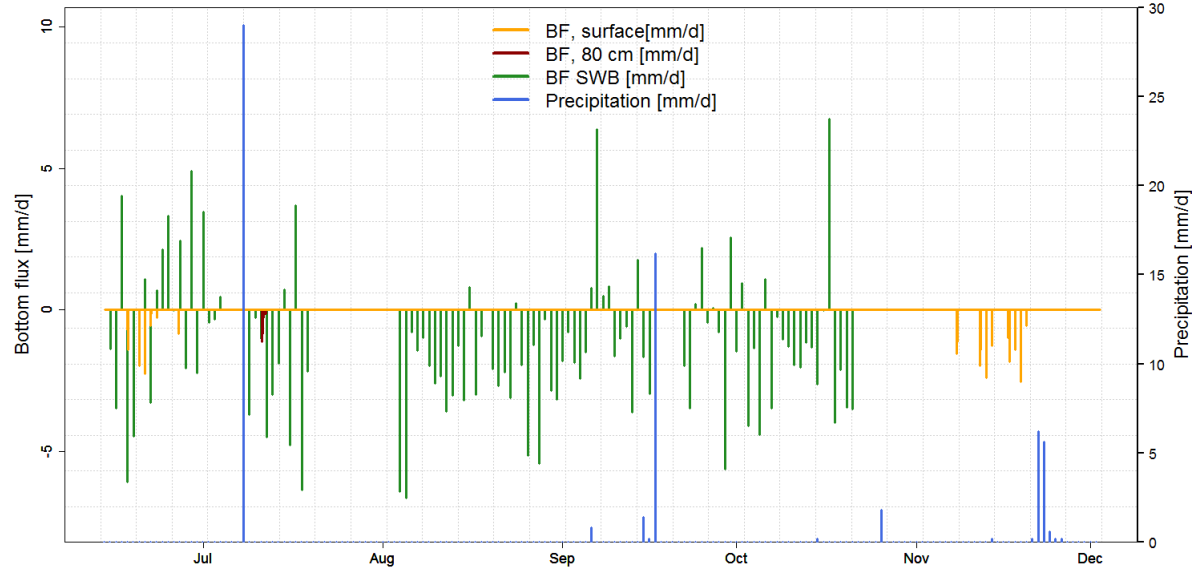
Relationship between incoming neutron intensity and CRS neutron intensity.

## Appendix II



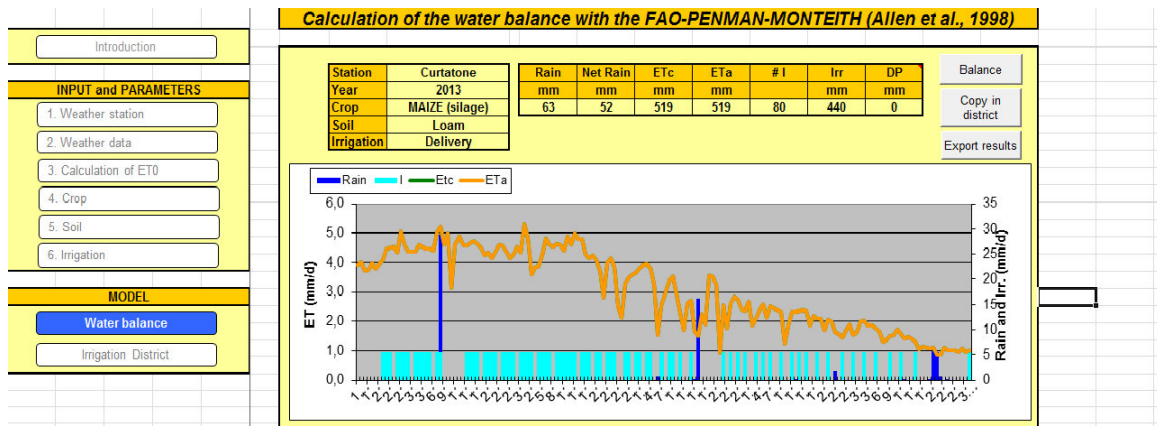
Meteorological parameter from June to December 2013 on the orchard: precipitation, temperature, relative humidity and net radiation.

## Appendix III



From SWB calculated bottom flux in comparison to the bottom flux, measured by the fluxmeter on the surface and in 80 cm depth.

## Appendix IV



Output of the Excel-sheet WatBal 3.0: actual and reference evapotranspiration, number of irrigations and its amount and deep percolation.



# **Declaration of Academic Honesty**

I hereby declare that the present thesis was written independently, without third party assistance and only with the usage of the sources, listed at the end of the work. Directly or indirectly thoughts, taken from foreign sources, are identified. Furthermore the thesis was not yet submitted officially or in another examination office.

Potsdam, 25.04.2014

Signature